UNCLASSIFIED

BSD-TDR-63-178

STRESS-TIME MEASUREMENTS IN HIGH VELOCITY IMPACT

by

S. M. Taylor, E. P. Palmer, R. R. Kadesch

UNIVERSITY OF UTAH
HIGH VELOCITY LABORATORY
Salt Lake City, Utah

Technical Report UU-13
Contract AF 04(694)-259

July 1963

Prepared for

AIR FORCE BALLISTIC SYSTEMS DIVISION
AIR FORCE SYSTEMS COMMAND
Norton Air Force Base, California

UNCLASSIFIED

HIGH VELOCITY LABORATORY
DEPARTMENT OF ELECTRICAL ENGINEERING
UNIVERSITY OF UTAH
SALT LAKE CITY, UTAH

UNCLASSIFIED

BSD-TDR-63-178

STRESS-TIME MEASUREMENTS IN HIGH VELOCITY IMPACT

by

S. M. Taylor, E. P. Palmer, R. R. Kadesch

UNIVERSITY OF UTAH
HIGH VELOCITY LABORATORY
Salt Lake City, Utah

Technical Report UU-13
Contract AF 04(694)-259

July 1963

Prepared for

AIR FORCE BALLISTIC SYSTEMS DIVISION
AIR FORCE SYSTEMS COMMAND
Norton Air Force Base, California

UNCLASSIFIED

ACKNOWLEDGEMENTS

The author is indebted to Dr. E. Paul Palmer, Associate Director of the High Velocity Laboratory, for providing the opportunity to pursue this research and for his helpful suggestions and enlightening discussions during the course of the experiments and the preparation of this thesis.

The author wishes to express his appreciation to Dr. Robert R. Kadesch for many valuable discussions.

A special debt of gratitude is here acknowledged to Dr. J. I. Swigart, Chairman of the Supervisory Committee, and Dr. T. J. Parmley, recently Chairman of the Department of Physics. Their constant encouragement and assistance throughout the author's entire graduate career has been a major factor in the achievement of this goal.

Sincere thanks is expressed to Dr. M. H. Miles for his friendly interest and help with the auxiliary experimental work with the composite oscillator, so essential to the analysis of the experimental data; to Warren L. Brown for his untiring work in the preparation and completion of the experimental detail work; to Earl F. Pound, of the Upper Air Research Laboratories for his technical assistance on the many problems associated with the electronic circuitry; to all other members of the staff of the High Velocity Laboratory for their help and encouragement.

Special thanks to Mrs. Joyce Hansen, Secretary of the Electrical

Engineering Department, for invaluable assistance during the research period, and in particular in the preparation of this manuscript.

The author wishes to express thanks to the Air Force Ballistic System Division, Air Force Systems Command for financial support for this research under the following contract numbers: AF 04(647)-176; AF 04(647)-942; and AF 04(694)-259.

The quiet and patient encouragement extended the author by his family has materially contributed to the completion of this work.

ABSTRACT

A new method for the measurement of stress-time effects in high velocity impact is outlined. A technique for mounting small barium titanate piezoelectric transducers within semi-infinite aluminum targets is described. The targets are impacted by spherical projectiles of the same material as the target. The projectiles were accelerated to velocities ranging from approximately 0.1 km/sec to 2.0 km/sec. The electronic circuitry developed to acquire information from the transducing elements is presented. The use of isotropic elastic theory in the analysis of the data thus obtained demonstrates that the experimental technique is, in fact, a suitable method for the measurement of these phenomena. It is demonstrated that the method will give significant information about wave propagation and stress levels in elastic and plastic waves. Further application of the system should provide more satisfactory information about the intricate, but still largely unknown, processes which attend the formation of craters in semi-infinite targets.

LIST OF FIGURES

TABLE OF CONTENTS

1. INTRODUCTION

There is little doubt that man's interest in the properties of the materials which compose the world in which he lives extends into antiquity. The practical problem of survival led to the discovery of materials which could be used for protection against the blows of his enemies. Down through the ages, one of the major problems man has faced is the continuing one of defense. Thus interest in the problem has been maintained. Each new development, from spears, arrows, body armor, gunpowder, and down to the present day rockets and satellites, has only served to make our interest just that more intense. In addition to this, man is a curious animal who will continue his interest in a problem solely to satisfy this curiosity.

The general problem still remains -- how to construct structures, etc., which will give protection under impact, more specifically, high velocity projectile impact. Thus when a projectile (sphere) is impacted against a target, a concentrated load of large magnitude is applied to the target, and the surface of the target is deformed as a result, this deformation in thick targets is called cratering.

The study of the phenomena associated with cratering has been the subject of extensive and intensive investigation ever since the introduction of gunpowder. Various investigators have devoted a great deal of effort and attention to the problems associated with the formation of craters.[1,2,3,4]

The investigator is struck by the apparent simplicity and symmetry associated with the craters. The final result has all the appearances of a frozen liquid, which solidified at some instant after a "drop" of liquid had struck its surface. This has led to many attempts to solve the problems by means of hydrodynamic theory. However, the assumptions required by the application of this theory, ultimately come down to the requirement of projectile velocities which have not been attainable until very recent time. Thus, the hydrodynamic approach would not seem to offer a productive avenue to a complete solution to the problem.

A variety of experimental techniques have been used to derive empirical relations to correlate crater characteristics with the properties of the materials used in the experiments.[5] The results of these investigations have met with limited success for the materials investigated and for the limited range of velocities considered. However, these empirical relationships cannot be extrapolated to new situations in the wider field of problems which require solutions.

An adequate model would solve the difficulty of this lack of generality. A general theory could be formulated from such a model. This would then give a description of the cratering process in high velocity impact, in terms of fundamental material properties and fundamental laws of the mechanics of deformable bodies. A knowledge of wave propagation assiciated with cratering would aid in the formulation and testing of this model.

A method for the determination of the characteristics of waves propagated in essentially semi-infinite targets, during the penetration or cratering process is presented in what follows. To do this, small barium titanate pressure transducers have been fabricated and embedded in the target or mounted on the target surface. These sensitive piezoelectric detectors have proved suitable for the detection of low-amplitude pulses, and they successfully indicate the time-amplitude history of low-level pulses. Their output characteristics in the presence of high-pressure pulses have not been previously investigated and the determination of these characteristics was one of the goals of this research.

2. THEORETICAL AND EXPERIMENTAL BACKGROUND

2.1 Wave Characteristics in Solids

Historical. The subject of stress waves is an ancient and well-established discipline when compared with some fields of applied mechanics. It is reliably reported that the propagation of elastic strains in a cylindrical bar subjected to tension impact had already been analyzed in 1807 by Thomas Young. Interest in the subject has waxed and waned to the present day. As a rough estimate, the "production rate" of papers on various aspects of this subject is currently well over one hundred papers per year. It is clearly impossible to cover the whole field under these circumstances. This brief review must be confined to some of the more relevant features of current

activity. The interested reader is referred to an excellent survey of the subject, edited by Batchelor and Davies, entitled, "Surveys in Mechanics," 1956, which contains extensive bibliographies.

While the study of stress waves has had a long and varied history, the major portion of this interest was narrowed to the study of the problems associated with the elastic properties of wire, rods, and bars. Very little work was done outside of these confines. Recently, more interest has developed in such subjects as plane-wave propagation in thin plates[6,7,8] and theoretical studies of the propagation effects associated with crater formation under high velocity impact.[9,10]

Elastic Waves. Hooke's Law for elastic distortion states that the stress (σ) is proportional to the strain (ϵ). The proportionality constant or modulus is dependent upon the particular strain involved. Thus, we have

$$\text{Young's Modulus:} \quad Y = \sigma/\epsilon = \left[(F/A)/(\Delta L/L)\right]$$

$$\text{Shear Modulus:} \quad \mu = \sigma/\epsilon = \left[(F/A)/\tan\phi\right]$$

$$\text{Bulk Modulus:} \quad B = \sigma/\epsilon = \left[(F/A)/(\Delta v/v)\right]$$

where:

F = Force

L = Length

ϕ = Angle of Shear

A = Area

v = Volume

Some solids may exhibit different properties in different directions,[11] however, our concern here is with isotropic homogeneous solids. These

solids possess both shear and volume elasticity. The shear elasticity involves distortion which gives rise to transverse (distortion) waves, and the bulk elasticity will give rise to longitudinal (dilatational) waves.

Mathematical analysis of the elastic wave problem[12] shows that the longitudinal wave in an extended isotropic solid medium propagates with a velocity

$$C_\ell = \left[(2\mu + \nu)\ (\rho_1)\right]^{1/2} \tag{1}$$

This can be written as

$$C_\ell = \left[(B + 4\mu/3)\ \rho_1\right]^{1/2} = \left\{\left[3B(1-\nu)\right] / \left[\rho_1(1 + \nu)\right]\right\}^{1/2} \tag{2}$$

using the relations

$$B = \lambda + 2\mu/3 \qquad (\mu = 0 \text{ for liquids})$$

$$Y = \lambda + 2(\mu - \lambda\nu)$$

$$\nu = \lambda/2(\lambda + \mu)$$

The transverse wave moves at a velocity

$$C_T = (\mu/\rho_1)^{1/2} \tag{3}$$

while for a long narrow rod, the velocity of a longitudinal wave becomes

$$C_L = (Y/\rho_1)^{1/2} \tag{4}$$

where

λ = a Lame's constant

ρ_1 = undisturbed density

ν = Poisson's ratio

We observe that the above velocities are dependent upon the moduli. If the moduli are constant, the velocities are constant and said to be sonic.

It is demonstrated in the literature[7], that a disturbance in materials will propagate with a velocity of

$$C = \left[(1/\rho_1) \ (d\sigma/d\epsilon) \right]^{1/2} \tag{5}$$

Thus, if the gradient of the stress-strain relation is constant, we see that such a disturbance travels at essentially constant speed -- the sound velocity. This should be true, regardless of the stress if the strain is less than the value at the elastic limit.

The above may be graphically demonstrated by means of Fig. 1, which displays the stress-strain relation for a typical elastic-plastic material.

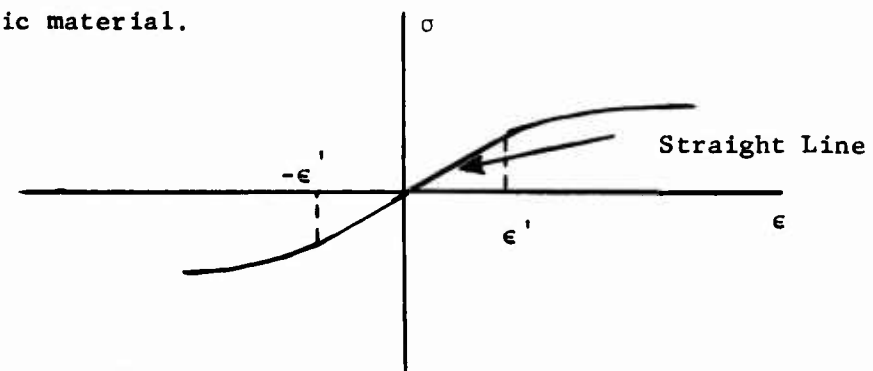

Fig. 1. Stress vs. strain relation for a typical elastic-plastic material.

The straight line between the two points $\pm \epsilon'$, the elastic limits, represents elastic deformation. It defines a constant modulus. The curve beyond the points $\pm \epsilon'$ represents plastic deformation. This part of the curve has a decreasing slope and therefore a decreasing modulus. Referring to Eq. 5, we see that materials which obey Hooke's Law, i.e., constant modulus ($d\sigma/d\epsilon$), will propagate a disturbance at a constant velocity. The same reasoning shows that a disturbance creating a strain greater than the elastic limit produces a plastic wave which would proceed at a subsonic velocity for the above case.

If the stress-strain curve were concave in the opposite direction, the plastic wave could become supersonic in either tension (first quadrant) or compression (third quadrant). Since this is a qualitative discussion we need not specify the particular type of strain involved because both volume strain and shear strain can be shown to be a combination of linear strains.

Shock Waves. The need for a precise definition of the term shock is indicated by the wide application of the term to various fields and phenomena, and the confusion which arises as a result of the variety of effects it is used to describe. If the stress-strain curve is concave downward in the third quadrant or concave upward in the first quadrant, the disturbance with the higher stress will move faster. This would create an infinitely steep leading edge on the pressure profile. There may be several other consequences resulting from this situation, but this infinitely steep leading edge is the only criterion

for a shock wave. We note that an elastic wave, where all pressure components move at the same velocity can never form a shock wave.

Another criterion is necessary to the definition of a stable shock; that is, the shock wave must travel at a velocity greater than that of the longitudinal elastic wave. This specification was added by Von Neumann. Thus, a disturbance in a solid can only form a stable shock when the elastic limit of the material is exceeded, and the stress-strain relation has the proper curvature noted above.

A further qualification of the preceding statement seems in order for solid materials: The intensity of the disturbance should be large compared to the shear strength, thus the shear modulus would be negligible ($\mu \triangleq 0$) and the material would behave virtually as a liquid.

The problem we are concerned with does not let us exclude the situation in which the shear modulus can be neglected. Thus, we include a qualitative discussion of the behavior of plastic waves in such solids.[13]

We consider the case for the longitudinal wave since it has a greater velocity than the transverse disturbance. The typical stress-strain curve for a solid in compression is given in Fig. 2, that is, provided

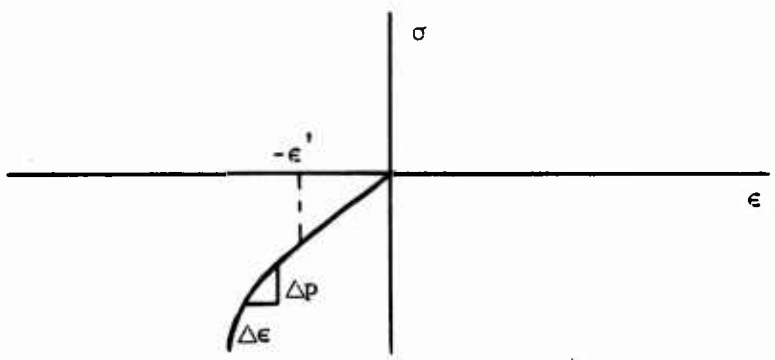

Fig. 2. Normal stress-strain curve for volume (bulk) compression.

the shear modulus is neglected. Figure 3 illustrates the variation of the shear modulus in compression. This latter complication must be

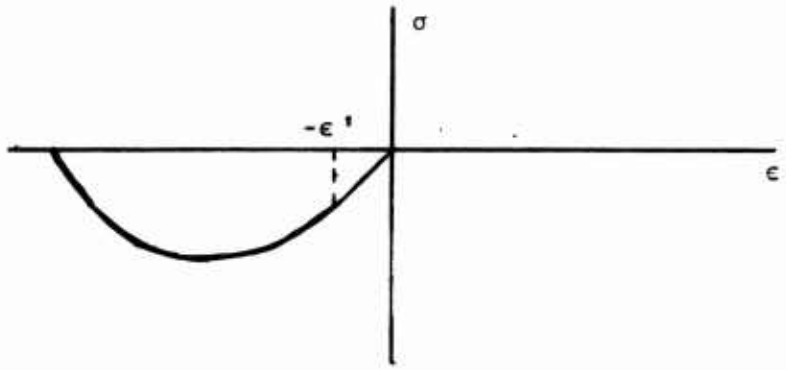

Fig. 3. Stress-strain curve (qualitative) for shear of a specimen in compression.

considered for purposes of our discussion.

We combine the qualitative curves for compression and shear from Figs. 2 and 3 according to the equation

$$C_\ell = \left[(B + 4\mu/3)\rho\right]^{1/2} \tag{2}$$

and obtain the composite curve of Fig. 4.

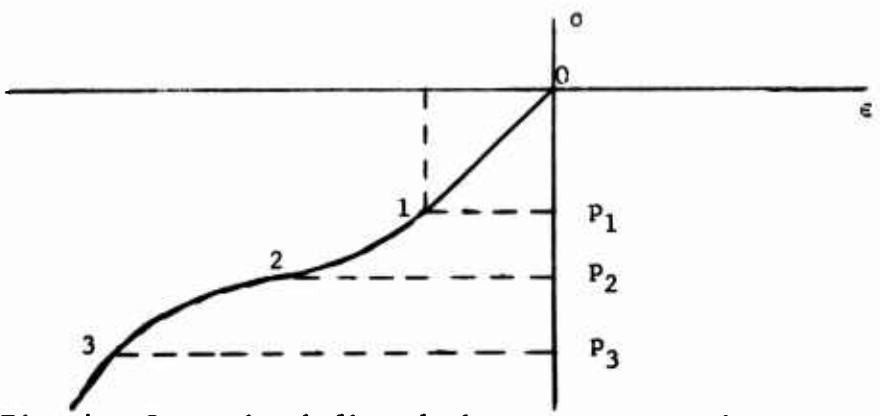

Fig. 4. Composite bulk and shear stress-strain curve

We now assume an initial wave of peak pressure (p), with a profile as indicated in Fig. 5(a). We also consider the idealized situation of no energy loss during propagation.

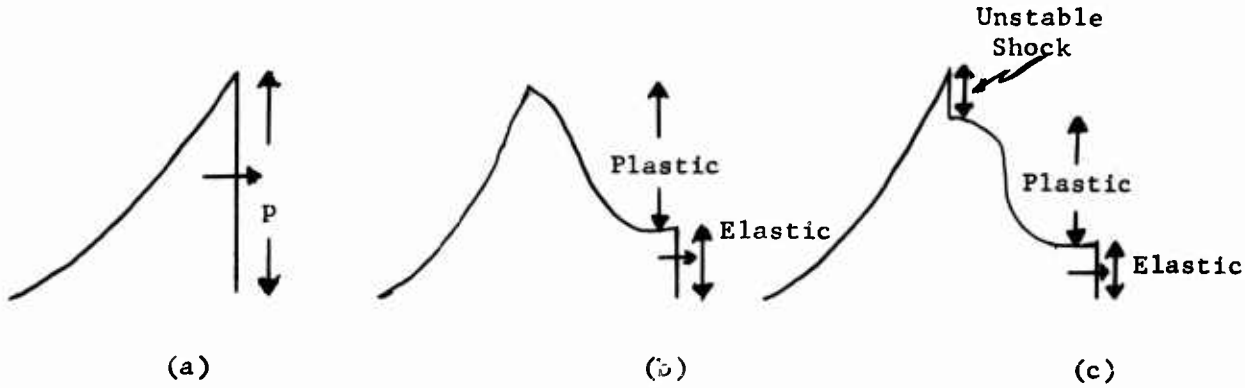

Fig. 5. Idealized pressure profiles in elastic-plastic materials, Refer to Eq. 2 and Fig. 4.

There are four cases which could develop:

1. $p < p_1$

   The elastic case. Low-velocity impact.[14] Here the pressure profile would not change from that shown in Fig. 5(a). Any slope that the applied pressure pulse developed upon application would remain constant.

2. $p_1 < p < p_2$

   The elastic-plastic case, (sometimes called shock wave deformation.[14]) After some arbitrary time interval, measured from the time of application of the pressure pulse, the pressure profile would have the appearance of Fig. 5(b). The elastic portion remains vertical and the peak pressure would lag further back with increasing

time, finally reverting to a flat topped sonic wave.

3. $p_2 < p < p_3$

The elastic-plastic case, also. Possibility of flow deformation. The front portion of the wave would have an appearance similar to the previous case. The pressure is larger and therefore the elastic part of the wave appears smaller. Point 2 of the curve in Fig. 4 is a point of inflection, thus the plastic wave velocity would increase for pressures greater than p_2. This would develop a shock, but not a stable shock, since the slope of the curve from 2 to 3 is less than that between 0 to 1. A flat-topped wave would appear when the pressure has decayed below p_1.

4. $p_3 < p$

The supersonic case. Figure 5(a) shows the pressure profile for this case. If the front were slanted rearward, it would become vertical with time, since it is a stable shock.

These idealized profiles are not likely to be realized in practice for the following reasons:

1. There is a very slow attenuation of elastic components in a wave.
2. Plastic components probably attenuate rapidly.
3. Shock components attenuate very rapidly.

With these considerations in mind, we can imagine an unsupported shock to experience the stages discussed. The high attenuation rate of the shock components is probably due principally to rarefactions over-running the shock.[7] The effects of shock or Hugoniot heating may also contribute to the attenuation.[6]

Summary of Wave Characteristics. The following effects could result from the mechanisms described above for any given single disturbance:

a. An elastic wave with a higher velocity than that of a plastic wave -- never slower.

b. An elastic wave with a higher velocity than that of an unstable shock -- never slower.

c. A plastic wave with a higher velocity than that of an unstable shock -- never slower.

d. A stable shock wave with a high velocity which allows it to engulf all other types of disturbances which may be preceding it.

The propagation of plastic waves in an infinite medium has been studied by D. S. Wood.[15] He used the assumptions of no change in density of the stressed material, that there are no strain-rate effects and that the material obeys the von-Mises/Hencky yield condition. The results of his calculations (for 24S-T aluminum) show that the velocity of the plastic wave of compression is about 0.8 times the longitudinal elastic wave velocity in the infinite medium. For a slender wire, this figure is 0.1 of the elastic wave velocity.

Radiation. The simplest nonplanar wave is a spherical wave. A simple source would be a radially pulsating sphere of diameter much smaller than the wavelength of the radiated waves. When the source is located in a free field, so that no waves are reflected back into the radiated sound field, the energy will be spread uniformly over a complete spherical surface at any radius from the source. At a radial

distance that is much larger than the wavelength or the source diameter, the wave front is essentially plane over distances comparable with the wavelength.

We describe the process in terms of the sound pressure as follows:

$$p = P_a(a)\frac{e^{j(\omega t - kr)}}{r} \tag{6}$$

where P_a is the pressure amplitude, a the diameter of the source, ω is the angular frequency of oscillation of the radiating source, $k = \omega/c = 2\pi/\lambda$, and r is the radial distance from the source. Note that c is the velocity of propagation of the sound and λ is the wavelength.

It is convenient to define a characteristic of the propagating medium. The specific acoustic impedance is defined as the complex ratio of the sound pressure to the particle velocity at a given point in a wave field. It is related to the mechanical impedance often defined in connection with the mechanical oscillator. Specific acoustic impedance is mechanical impedance per unit area. One can write

$$Z_{sp} = \rho_o c(\phi) \tag{7}$$

The impedance function ϕ is determined by boundary conditions and by the point in the wave at which the impedance is designated. When $\phi = 1$ (a free plane-wave, no returning wave) the specific acoustic impedance is equal to $\rho_o c$. This is called the characteristic impedance

of the medium. The cgs unit is the "rayl" ($g/cm^2/sec$. The characteristic impedance is a pure resistance, and this says that in the case of free waves, the energy is continually drained away into a radiation resistance and there is no reactive component in the "circuit."

We return now to our simple spherical wave source The specific acoustic impedance of this situation can be shown to be:[16]

$$Z_r = \frac{\rho_o c}{1 + (1/jkr)} = \frac{1}{(1/\rho_o c) + \left(\frac{1}{j\omega\rho_o r}\right)} \qquad (8)$$

Now, if $kr >> 1$, i.e , $r >> \lambda$, the spherical wave correction term containing jkr vanishes. The specific acoustic impedance becomes a pure resistance, and we have the condition of a free plane-wave. As an example, it may be noted that for a distance of 50 m and frequency of 1000 cps, the impedance given by Eq. 8 is within 1 per cent of the plane-wave value.

It is worthy of note that the problems of radiation are described by the same mathematical expressions and the same physical concepts whether one is discussing sound radiation or electromagentic radiation. Thus one can talk about the Fraunhofer diffraction in the 'far field', where the plane-wave is propagating, and also, the 'near field' may be analyzed for Fresnel diffraction. These terms are popularly associated with light or electromagnetic diffraction effects, but they have equal applicability to the problems of sound radiation.

Reflection and Transmission Coeffieients. We frequently deal with a system of two or more different substances carrying sonic energy.

Thus when a wave strikes a boundary, there is, in general, a reflected wave. A certain fraction of the incident pressure will also be transmitted into the medium on the other side of the boundary.

The waves at either side of the boundary must satisfy two boundary conditions:

1. The total pressure must be the same on both sides.
2. The particle velocity into the boundary must equal the particle velocity out of the boundary on the other side.

If waves originate in the first medium only, in which $Z_1 = \rho_1 c_1$, and the waves transmitted into the second medium, where $Z_2 = \rho_2 c_2$, travel away to infinity without reflection, we can write:[16]

$$\frac{P_{1-}}{P_{2+}} = \frac{r-1}{r+1} \quad \text{(normal incidence pressure reflectivity)} \qquad (9)$$

$$\frac{P_{2+}}{P_{1+}} = \frac{2r}{r+1} \quad \text{(normal incidence pressure transmissivity)}$$

where $r = Z_2/Z_1$, and the P represents the pressure amplitude, with the positve and negative signs used to indicate the direction of propagation of that particular pressure amplitude.

We are often more interested in the energy exchanged upon reflection and transmission. Thus, using the above relationships, it is a simple matter to show:

The reflection coefficient is:

$$\alpha_r = \frac{I_{1-}}{I_{1+}} = \left(\frac{r-1}{r+1}\right)^2 \tag{10}$$

The transmission coefficient is:

$$\alpha_t = \frac{I_{2+}}{I_{1+}} = \frac{4r}{(r+1)^2} \tag{11}$$

where the I represents the intensity of the radiation. In general r, Z_1, Z_2, and the reflectivity and transmissivity are complex quantities, though in many practical problems they are real.

2.2 Experimental Measurements

The previous discussion considered the propagation of a disturbance through a solid in terms of either a strain propagation or a stress (pressure) propagation. In order to study these effects, it is necessary to have a detector of some sort which will react to either of these effects.

There are several physical phenomena which might be used for this purpose. It is known that the resistance of a material will change under the effects of pressure. The resistance of a conductor will change with elongation. This latter effect is the basis for the operation of the well-known strain gage. The name of the strain gage indicates its use, i.e., detecting the change in strain.

There are several materials, such as quartz, Rochelle salt, barium titanate compounds, etc., which are piezoelectric. A piezoelectric (pressure-electric) substance possesses a useful combination of electrical and mechanical properties. A suitably prepared piece with conducting electrodes on one pair of faces behaves like an electric capacitor. At the same time, the material behaves like a mechanical spring with an internal stiffness that opposes an applied force. In addition, piezoelectric materials exhibit a special behavior in which electric charges are produced by straining the material and, conversely, internal forces are produced by subjecting the material to an electric field. These forces produce a strain. In general, since the material acts as a capacitor, the charges produced by a strain will develop a voltage across the material.

A piezoelectric detector, when placed in the path of propagation of a stress wave, would be compressed; i.e., strained, and a voltage would be developed. With suitable electronic instruments, this voltage can be used to determine the arrival time of a stress wave. Furthermore, since the voltage developed is directly proportional to the force applied (See Appendix II), the possibility presents itself of making a measurement of the magnitude of the force(s) associated with a propagating stress wave.

The choice of barium titanate as a detector for the purpose of this experiment was dictated by its superior mechanical ruggedness and the availability in any desired shape. The piezoelectric effect is temperature dependent. Any given material will cease to exhibit this

property if its temperature is raised above a certain critical level called the Curie point. Barium titanate possesses the best stability over the temperature ranges contemplated for conducting this experiment (ambient temperatures up to 105° F.) The material also possesses moderately good piezoelectric properties when compared with other materials, such as quartz, Rochelle salt, etc.

Barium titanate ceramic piezoelectric detectors are fabricated in a wide variety of sizes and shapes. It was possible to obtain the detectors from a local manufacturer.[17] The mechanical and electrical properties could be specified in accordance with the capabilities of the manufacturer, and in conjunction with their research department. Thus it was possible to obtain extremely small units to be inserted into the target with the least possible damage to the integrity of the target.

A survey of all the cratering experiments conducted at this laboratory indicates that these transducers can be inserted into the target from the back and positioned at a desired distance from the front, or impacting surface, and not disturb the integrity of the target as far as the cratering process is concerned. This is true if the target is properly supported so as to act as a semi-infinite solid. In other words, it appears that the cratering process is an extremely localized effect, in a properly mounted target.

A typical value for the output of these transducers, as given by the manufacturer, is 20×10^{-3} (Volts/m)/(Newton/m^2). That is, volts per meter of length when a force in Newtons is applied to the area of the transducer which is perpendicular to the length dimension. Variation

Best Available Copy for the next page

teristics

were fabricated locally.[17] The

a transducer with the greatest

ngth and "best" sensitivity commen-

The size, noted below, was the small-

produced with realiability and uni-

the following properties:

to within a few thousandths

an inch)

e/m^2 lb

2.14×10^3 Kg/m^3 (measured value)

(Ref. 16, p. 247)

Longitudinal Sound Velocity: 4.43 mm/μsec (average of measured values)

Acoustic Impedance: 24.6×10^6 Kg/m^2-sec ($Z = \rho c$) (Calculated value)

Curie Temperature: 120° C. (Ref. 18)

Dielectric Constant: 1400 (approximate) (Ref. 17)

Dielectric Strength: 150 volts/mil thickness (minimum) (Ref. 17)

Capacitance: 21 pf. (approximate) (Ref 17)

Nominal output: 25×10^{-5} (Volts/m)/Newton/m^2 (See Appendix II)

The value for the nominal output represents the output in volts per meter of length when a force in Newtons is applied to the area of the transducer which is perpendicular to the length dimension. The above value is the average value for six (6) different, randomly selected transducers or crystals. These crystals were used in three different calibration methods, as outlined in Section 3.9 and Appendix II.

The transducers (sometimes called crystals) are polarized in the long dimension. Both of the square ends are silvered and a wire lead is attached to the negative electrode surface. The units have a moisture proof cover, except for the positive electrode surface, which is clean and ready for electrical connection. See Fig. 6.

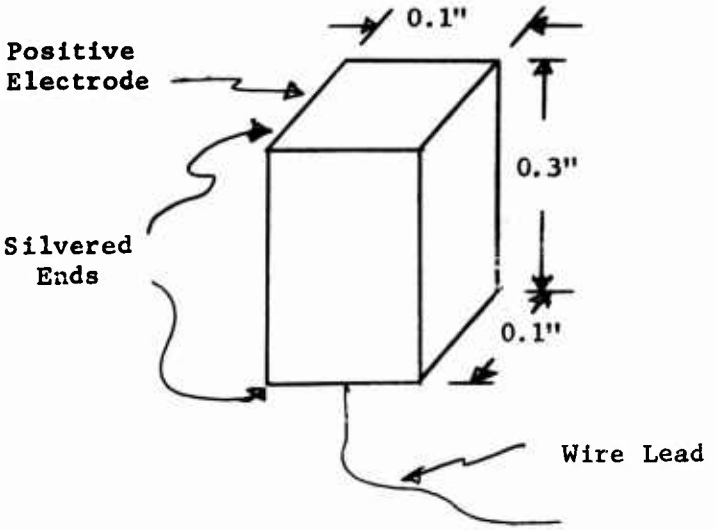

Fig. 6. Sketch of barium titanate transducers.

The physical properties and piezoelectric mechanism of barium titanate transducers are covered in more detail in Appendix II.

3.2 Target Characteristics

The targets were cylinders of un-annealed 1100-F aluminum having a diameter of 10.16 cm. (4 inches) and a length of 5 cm. The two end surfaces were machined smooth and parallel.

The following properties of the 1100-F aluminum were determined with standard testing techniques and machines under what might be termed semi-static conditions.

Yield Stress: 4.57×10^8 dynes/cm^2

$6{,}640$ lb/in^2 (compression)

* Elastic Modulus: 7.012×10^{11} dynes/cm^2 (Young's Modulus, compression)

10.17×10^6 lb/in^2

Density: 2.740×10^3 Kg/m^3

Brinell Hardness Number: 23-24

* Poisson's Ratio: 0.297

* Longitudinal velocity of sound: 5.85 mm/μsec (Handbook value[20] $6.42 \frac{\text{mm}}{\mu\text{sec}}$)

Acoustic Impedance: 16.03×10^6 Kg/m^2-sec [20] (longitudinal)

* (Obtained using composite oscillator, see Appendix II.)

3.3 Target Mounting

A special target holder and mounting device was designed and built for use in the tunnel firing range of the laboratory. It is shown in cross-section in Fig. 7. It is designed to make it possible to position the target with some degree of facility and accuracy in both horizontal and vertical directions. A small hole, large enough to insert a couple of fingers, is cut in the back portion of the target holder. This is not shown in the sketch. This hole allows one to manipulate the wire lead from the transducer with greater ease without the necessity of disturbing the position of the target holder itself. The entire

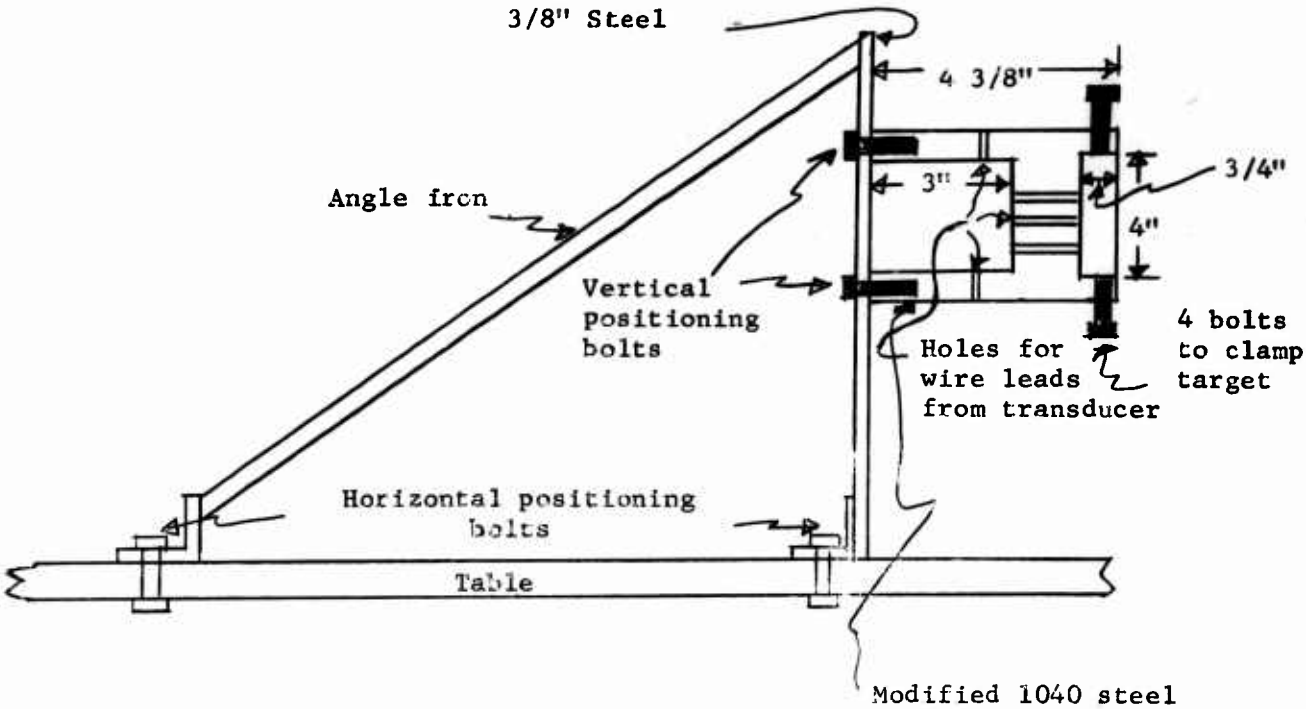

Fig. 7. Target holder and mounting device.

assembly is bolted to a heavy angle-iron frame which is in turn firmly bolted to the concrete walls of the tunnel in which the firing range is situated. The combined effects of the choice of target thickness and mounting device serve to supply a target which is essentially semi-infinite in nature -- as far as the experiments reported here are concerned.

3.4 Target Preparation

A hole, 9/64 in (0.1406 in) diameter, is drilled in the aluminum target to the desired depth, then a specially prepared drill, with the

same diameter, is used to make the bottom of the hole flat.

The problem of binding the transducers in the target was explored at great length. After experimenting with several glues, epoxy's. epoxy loaded with metal, etc., the choice devolved upon a eutectic mixture of tin-silver-mercury used by dentists to fill cavities in teeth. This choice was influenced by the following considerations: The amalgam is electrically conductive; when it is properly prepared, it expands slightly upon setting, and it has an acoustic impedance very near that of the barium titanate (see below).

The amalgam or filling alloy used was obtained from a local dental supply house. Since the properties of this amalgam vary somewhat from one manufacturer to another, the amalgam used in these experiments is specified as follows: Hammonds Argentum Filling Alloy, Fine Cut, with 12 grain Alloy Capsules, and 18 grain Mercury Capsules.

The contents of one of each of these capsules is placed in a mortar and pestle and mixed according to the manufacturer's instructions. A small amount of this amalgam is placed in the bottom of the hole, using a dental probe of small diameter. The wire lead from the transducer is threaded through a 1.5-2.0 x 10 mm., "Kimax"* glass melting point capillary tube. This glass tube is used to push the transducer into the hole and make a good contact with the filling alloy while it hardens -- approximately 2 to 3 minutes. The filling alloy will harden rather

*Kimble Glass Co., A Subsidiary of Owens-Illinois General Offices, Toledo, Ohio.

fast, so a certain amount of efficiency must be used in order to carry out this procedure and obtain a good bond to the target.

There are two reasons for using small amounts of the amalgam:

a. To prevent an electrical short circuit between the two ends of the transducer.

b. To keep the thickness of the layer between the transducer and target as small as possible.

The amalgam was allowed to set for a minimum period of 24 hours before any tests were made as to the effectiveness of the bond. It is known that the amalgam attains approximately 90% of its compressive strength after this period of time.[21]

When a transducer has been properly seated in the target, the remainder of the hole is filled with a wax. This wax is known as "sticky wax," also used by dentists. It is melted to a consistency which allows it to be used to fill the remainder of the hole. The melting point of the wax is between 40°C. and 50°C. The Curie temperature of the barium titanate is 120°C., so the transducers are not endangered by this process.

The apparatus shown in Fig. 8 is used to heat the "sticky wax." It allows the wax to be melted sufficiently to fill the hole without the necessity of heating the entire target. The heating element can be inserted into the hole between the glass tube and the wall of the hole. This makes it possible for the melted wax to flow more easily into position around the transducer.

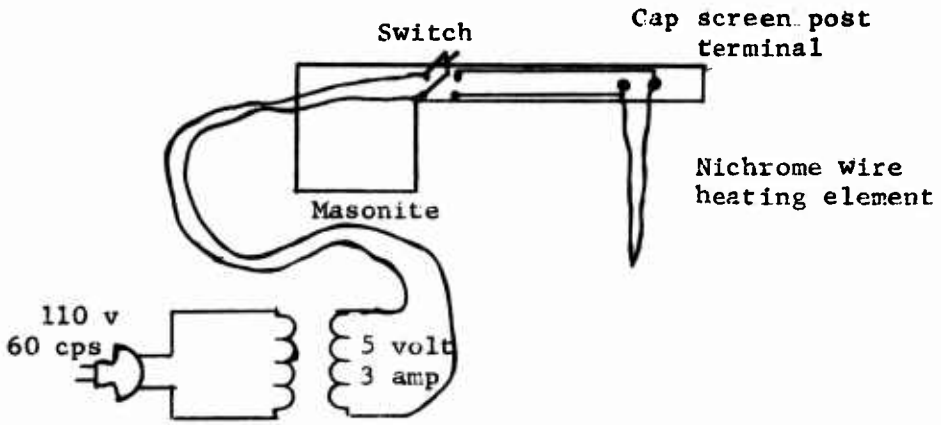

Fig. 8 Heating device for "sticky wax," used in target preparation.

A schematic cross-section of a completed target-transducer assembly is shown in Fig. 9. The transducer is positioned at various distances (d) from the front or impact surface. The wire lead is attached to the

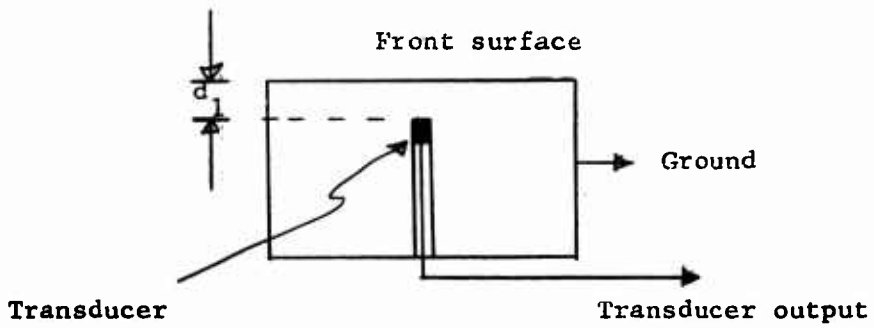

Fig. 9. Schematic cross-section of target-transducer assembly.

negative electrode of the transducer, which in turn is connected to the electronic circuitry. The positive electrode makes electrical contact through the amalgam, the target forms the common "ground" for the circuitry.

An idealized schematic cross-section of the transducer as mounted in the bottom of the hole is shown in Fig. 10.

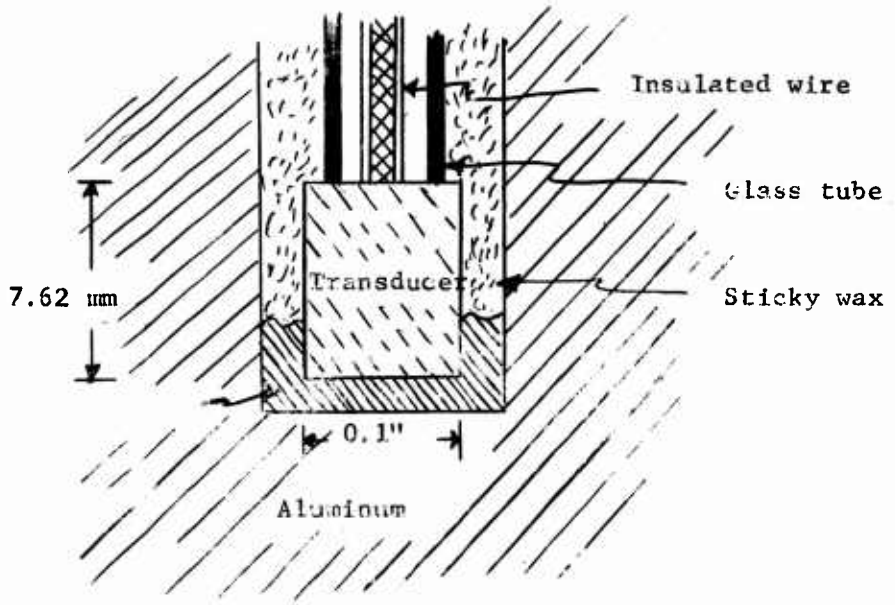

Fig. 10. Schematic cross-section of the mounted transducer. (Idealized)

3.5. Properties of the Tin-Silver-Mercury Amalgam

The literature[21,22] gives the following values for some of the physical properties of the amalgam used in these experiments. The average modulus of elasticity is given as 0.965 - 1.24 x 10^{11} dynes/cm^2 (1.4 - 1.8 x 10^6 lb/in^2). The average compressive strength is given as

3.1×10^9 dynes/cm^2 (4.5×10^4 lb/in^2). The proportional limit has been found to be between 70% to 80% of the compressive strength.[22]

Attention is directed to the fact that if greater pressure is exerted on the amalgam when it is being put into place -- the dental term is "condensation" -- the above value for the compressive strength will increase.

The following properties of the amalgam were determined by measurements made on samples prepared here in the laboratory

Density: 12.34×10^3 Kg/m^3

Longitudinal Velocity of Sound: 2.13 mm/μsec

Acoustical Impedance: 24×10^6 Kg/m^2-sec ($Z = \rho c$)

Logarithmic Decrement: 4.8×10^{-3} (δ)

The logarithmic decrement (δ), (16, p. 321), is the most common of several quantities used to describe the magnitude of internal friction. Internal friction is defined as the capacity of an isolated vibrating system to dissipate mechanical energy into heat. For internal friction studies, δ is usually defined as the natural logarithm of the ratio of any two successive amplitudes in a system undergoing free decay.

The measurements of the logarithmic decrement and the velocity of sound were conducted in the Solid State Physics Laboratory of the University of Utah. The device used was a composite oscillator of

the type described by Marx[23] and Seely,[24] and is fully described in Appendix I.

3.6. Epoxy Binding Agent

A new bonding agent was discovered near the end of the testing program. Prior to this event the epoxy method of binding the transducers in the target was abondoned because, the exothermic chemical reaction of the materials in the epoxy cements available, generated temperatures well in excess of the Curie temperature of the transducers.

This epoxy-type binder is available from the Hysol Corporation, Olean, New York, and South El Monte, California, in their "Expoxi-Patch Kit." The curing temperature of the epoxy bonding agent is approximately the same as room temperature. Thus the transducers will not be damaged by heat effects, since their Curie temperature is 120°C. (248° F.).

This new bonding agent is attractive because it allows the transducer to be positioned very close to the target material, at the bottom of its hole. It also allows a simplification in the analysis of the data.

Two targets were prepared with this new binding agent.

3.7. Projectile Characteristics

The spherical projectiles used were commercial balls[25] having a diameter of 5.55 mm (7/32 in.), and a mass of 250 milligram. The analysis given by the manufacturer is: copper 4.0%, magnesium 0.5%, manganese 0.5%, with the balance aluminum.

The mechanical properties are:

Modulus of Elasticity: 7.16×10^{11} dynes/cm^2

10.4×10^{6} lb/in^2

Yield Strength: 2.76×10^{9} dynes/cm^2

40,000 lb/in^2

Density: 2.79×10^{3} Kg/m^3 (measured)

Brinell Hardness Number: 86-87

3.8. Electronic Circuitry

1. Attenuator and Cable Coupling Circuit. The magnitude of the output pulse obtained from the transducers in preliminary experiments indicated the need for some sort of attenuator network which would preserve the integrity of the pulse with respect to both amplitude and rise-time. The capacitance compensated resistor-divider network, shown in Fig. 11, was chosen, since it will not be affected by the frequency of the signal if the following condition[26] is met: $R_1C_1 = R_2C_2$, and the voltage transfer function becomes: $e_o/e_i = R_2/(R_1 + R_2)$.

   The following voltage ratios were chosen: 1/10, 1/100, 1/1000,

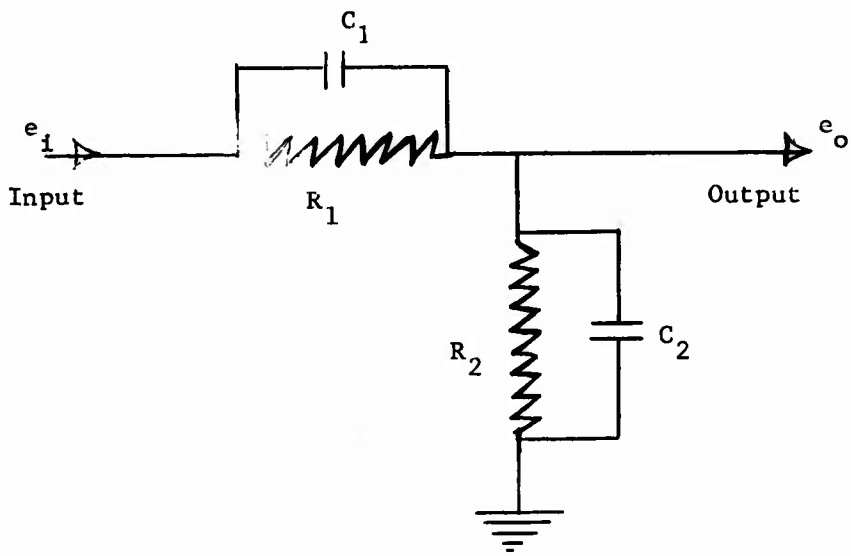

Fig. 11. Capacitance compensated resistor-divider network.

1/10,000. More complete information concerning the attenuators used in the experiment, including circuit schematics, will be found in Appendix IV.

2. White cathode-follower. An impedance transformer of some sort is necessary in order to couple the signal from the high impedance attenuator to the low impedance (50 ohm) coaxial cable. A modified "White" cathode-follower circuit was chosen for this purpose. A generalized electrical schematic of this circuit is shown in Fig. 12.

The White cathode-follower is a two-tube series device that provides output impedances of the order of 5 ohms and transmits pulses of either polarity with minimal distortion.[27]

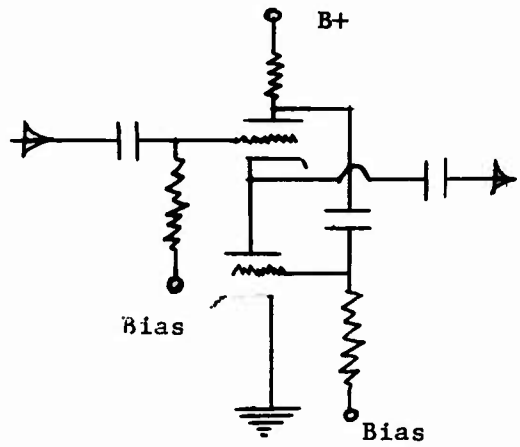

Fig. 12. Generalized electrical schematic of White cathode-follower.

A more complete discussion of the particular circuit used in this experiment will be found in Appendix IV.

3. Velocity Measuring System. The velocity measuring system consists of a Berkeley Model 7360 EPUT Meter used as a Time Interval Meter (TIM) to record elapsed time.

A schematic diagram of the pulse forming network and aluminized mylar-plastic film switches[28] is shown in Fig. 13. The mylar sheets are placed in the path of the projectile in the role of a switch. A potential is applied across the mylar insulator. When a projectile perforates the mylar sheet, the switch is closed, thus causing a capacitor to discharge through a resistor. The pulse either starts or stops the TIM. The TIM indicates the time of flight between two mylar sheets in micro-seconds. The information from the counter is used to calculate the average velocity of the projectile after the distance between the two

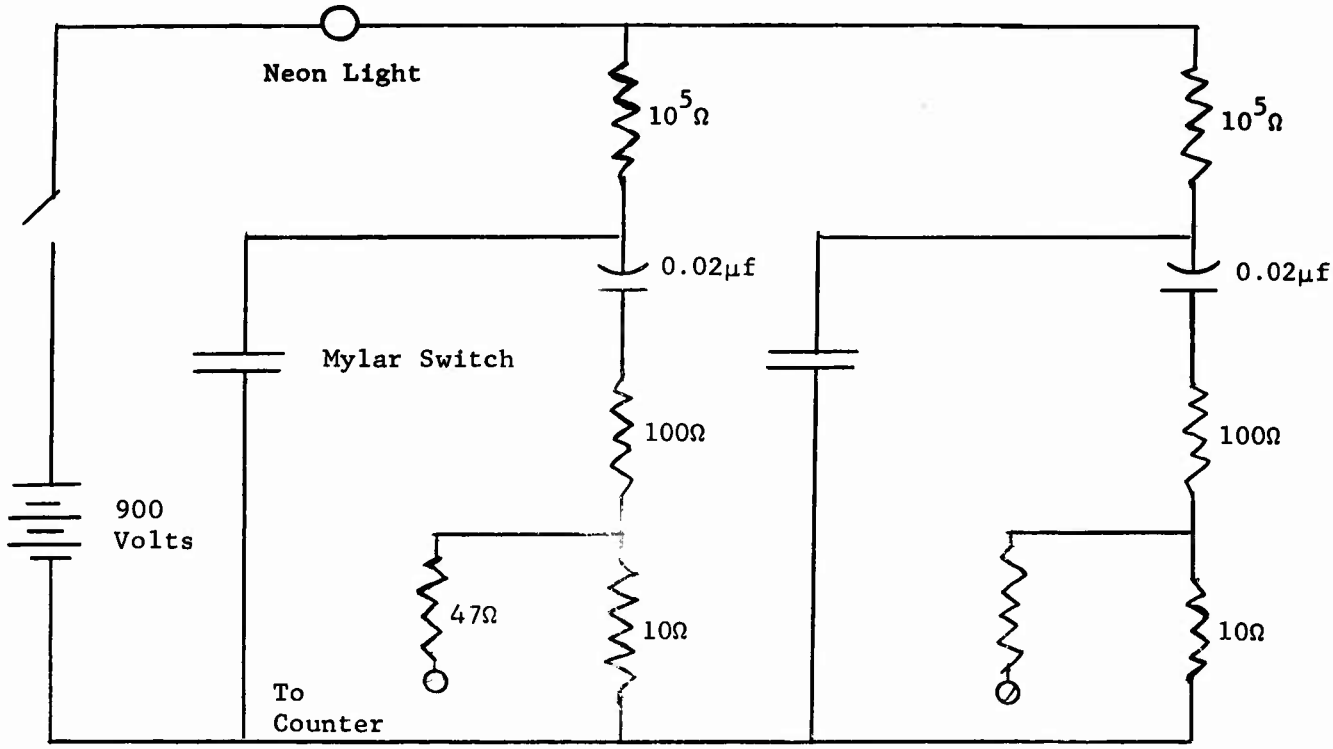

Fig. 13. Schematic diagram of pulse-forming network and mylar switches.

mylar sheets has been accurately measured. The pulse output of the circuit is approximately 80 volts with a rise-time less than 0.05 micro-second.

4. Impact Time Trigger Circuit. A triggering pulse is required to start the sweep circuits of the oscilloscopes which are used to record the output of the transducers during the experiments. The circuit, shown in schematic in Fig. 14, represents the first successful solution to this problem. Regular commercial aluminum foil is stretched between two posts with sufficient tension

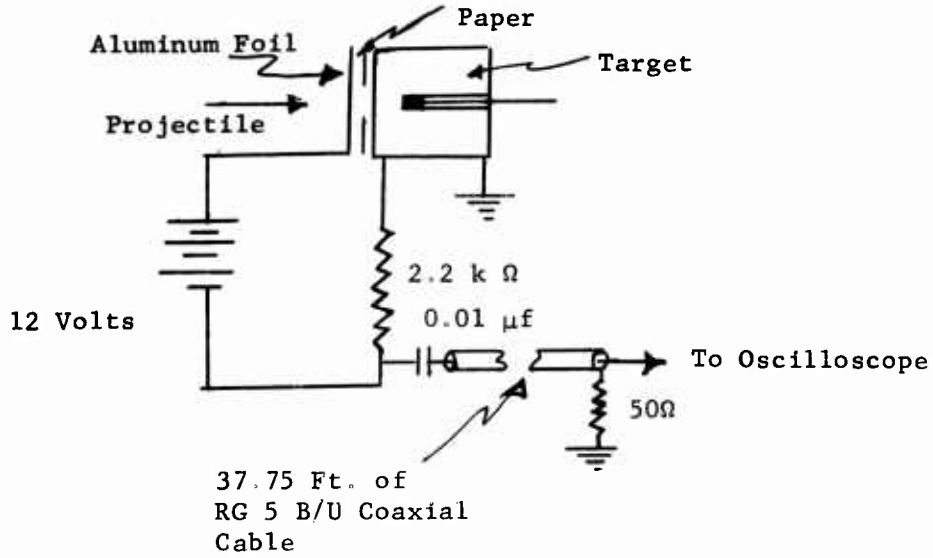

Fig. 14. Impact time trigger circuit

to make a flat surface and still not change its dimensions. It is insulated from the target by a thin piece of paper (approximately 0.005") which has a 1 inch diameter hole cut in it over the point of impact. When the projectile hits the target, the aluminum foil contacts the target, completing the circuit. The voltage developed across the resistor is then used for the trigger pulse. The rise-time of this circuit has been measured to be approximately 0.04 to 0.08 micro-seconds.

The results obtained in the first series of tests, seemed to indicate that the foil was making contact with the target prior to impact -- especially for the low velocity shots. This was remedied by placing a piece of thin tissue paper between the target and aluminum foil. There is no hole in the

tissue paper. The projectile perforates the foil and the tissue paper, and the circuit is completed between the foil and target by means of the projectile itself. The completion of the circuit generates the desired initial pulse. Note that the tissue paper is the only material between the aluminum foil and the target.

5. Integrated System. A block diagram of the complete electronic system is shown in Fig. 15. The two different lengths of cable

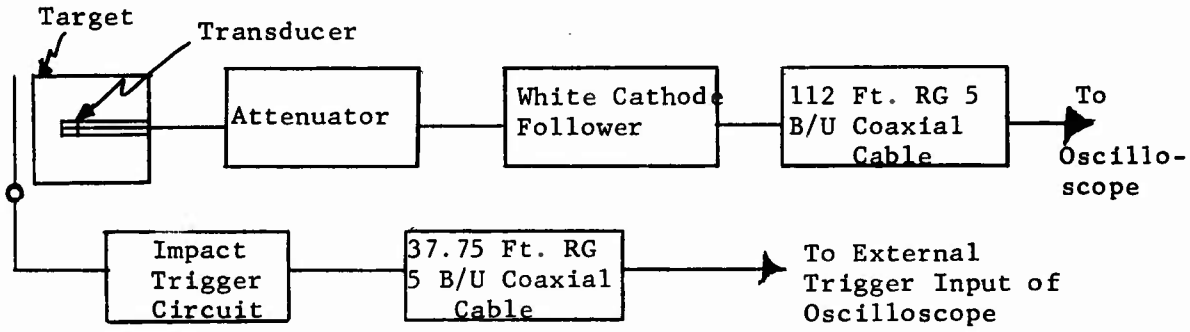

Fig. 15. Block diagram of complete electronic system.

are used to ensure that the oscilloscopes will have their sweep circuits in operation when a signal arrives from the transducer.

The measured time delay for the same signal to transverse the two signal pathways shown in Fig. 15 was found to be 0.13 micro-second. The rise-time (10% - 90%) of the attenuator and cathode follower system was measured and found to be 0.03 to 0.05 micro-second. The time delay of the signal in passing

through this latter system was measured and found to be 0.08 to 0.09 micro-second, and its decay time constant is approximately 200 micro-seconds -- depending on the particular attenuation ratio used in the circuit.

3.9. Calibration

There is sufficient variation in the characteristics of the transducers that each one should be separately calibrated. One test was conducted to gain some information relative to the uniformity of the transducers. The first mechanical resonance was determined when the transducer was driven by a constant voltage variable frequency signal generator. Details of the test set-up are shown in Appendix III. The results of this test showed that the variation in the frequency of this first mechanical resonance was less than 6.4%, about a mean of 290,818 cycles per second.

1. Free-Falling Ball Test. An attempt was made to obtain information on the output of the mounted transducers by dropping a ball from various heights onto the target-transducer assembly. The ball was held by an electro-magnet, dropped through a 4-inch, close-fitting launch tube, (used for aiming purposes) onto the target. It was found that it was not possible to hit the target with the required accuracy from heights as low as 0.25 meter.

   A similar test was arranged, using a pendulum on a thin stiff rod rather than attempt a redesign of the above experiment. Here

again, it was found that the output of the transducers was highly dependent upon the point of impact relative to the position of the transducer in the target. It was necessary to use a guide channel to make the pendulum ball hit the target at the desired position. The pendulum was no longer falling freely under these circumstances, but it was possible to measure the velocity of the pendulum just prior to impact. The results of this test confirmed that the point of impact has a material bearing on the output of the transducer.

2. Projectile Impact Calibration. Another attempt at gaining some information as to the output of the transducers involved the use of a firing range. The technique of firing the gun was developed to allow a wide range of impacting velocity. This was done using both powder explosives and compressed air to accelerate the projectile. Each target was subject to a low velocity of approximately 0.1 km/sec and then to a selected higher velocity. The low velocity is such that the projectile just barely forms an impression in the face of the target -- 0.2 - 0.3 mm. Early test results gave little indication of success for this method.

3. Semi-static Measurements. This method was recommended by the manufacturer.[17] The transducer is connected in parallel with a capacitor of approximately 210 pf which is ten times the capacitance of the transducer itself. A mechanical load is

placed on the transducer, the system is discharged, and then the load is quickly removed. The change in the voltage of this system (two capacitors in parallel) is then measured. A very high input impedance instrument, such as an electrometer, is needed to make this measurement. Measurements were made on three different transducers and an average value was taken in each case. The results are reported in Appendix II.

4. Dynamic Measurements -- Rod Impact Experiment. This method involved the comparison of the output of the transducer with that of a strain gage. The transducer was fixed on the central axis of a specially prepared aluminum (2024-T4) rod. That is, the transducer was placed within the rod itself. A strain gage was fixed on the outside of the rod, immediately in front of the position of the transducer. See Fig. 16.

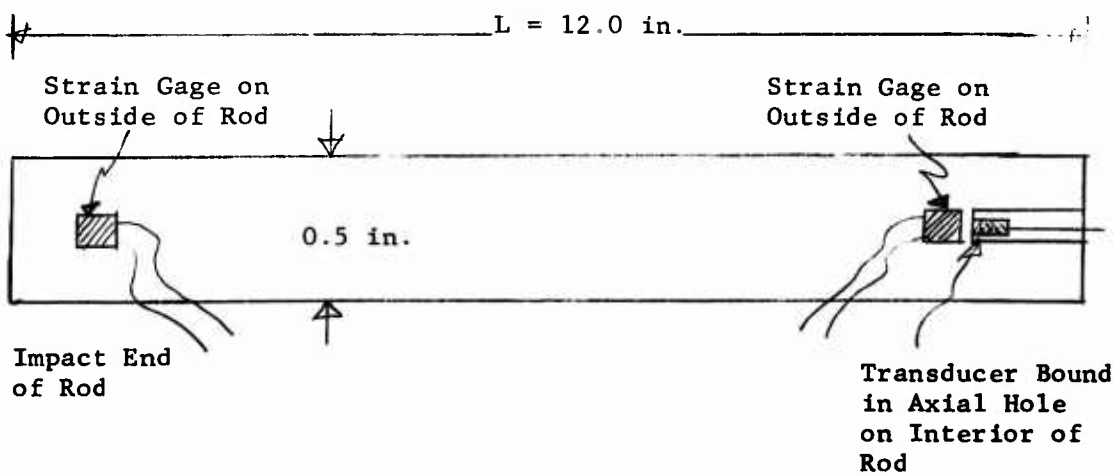

Fig. 16. Sketch of location of strain gages and transducer for rod-to rod impact experiment.

The data developed by the two strain gages were used to calculate the propagation velocity through the rod, which was used as a further check on the rod impact experiment as well as on the operation of the transducers.

This rod was placed in an experimental apparatus, developed in the High Velocity Laboratory,[29] to study the effects of stress wave propagation in a system of two rods, one impacting the other. The velocity of the impacting rod was kept at a low enough value to insure that the elastic limit of the rod material was not exceeded -- for this experiment.

The output of the strain gages and the transducer were displayed on oscilloscopes and photographic records made of the voltage pulses thus obtained. The transducer output was fed through the same electronic system as described above. The horizontal sweep circuits of the oscilloscopes were triggered by a signal which was generated upon impact of the rods. The output of the strain gage was used as a means to determine the stress at the location of the strain gage and transducer. This information was then used to determine the output characteristic of the transducer. Agreement with the results of the Semi-static Measurements was quite good and is reported in Appendix II.

Two separate rods were prepared and used in this experiment. The transducer was fixed in position with amalgam in one rod, and with the epoxy cement in the other rod. As a further test

of the data of this experiment, the output characteristic (volts per unit stress) determined from one rod was used to convert the voltage output signal of the transducer in the second rod to a stress value. This stress value was then compared with that obtained from the strain gage mounted on that same (second) rod. These values compared very well, to within a factor of two.

5. Dynamic Measurements -- Composite Oscillator Tests. The output of a transducer was obtained in a vibrating system, known as a composite oscillator, and referred to above in Section 3.5., and more fully described in Appendix I. The output signal of the transducer was used in conjunction with the data available from the composite oscillator to determine the output characteristic of the transducer. The agreement with the value obtained in the previous two tests was excellent.

3.10. Integrated Experimental System.

Figure 17 is a schematic diagram of the complete experimental system, including the projectile-acceleration and velocity-measuring systems.

The gun is a specially designed, smooth-bored gun chambered for 220 Swift cartridges. The shells are hand loaded with desired powder combinations and weights. The gun is fired by means of a solenoid-drive firing pin when the projectiles are accelerated with explosive powder. It is fired by means of a solenoid-operated valve when the compressed air is used to accelerate the projectiles. As a safety precaution, the

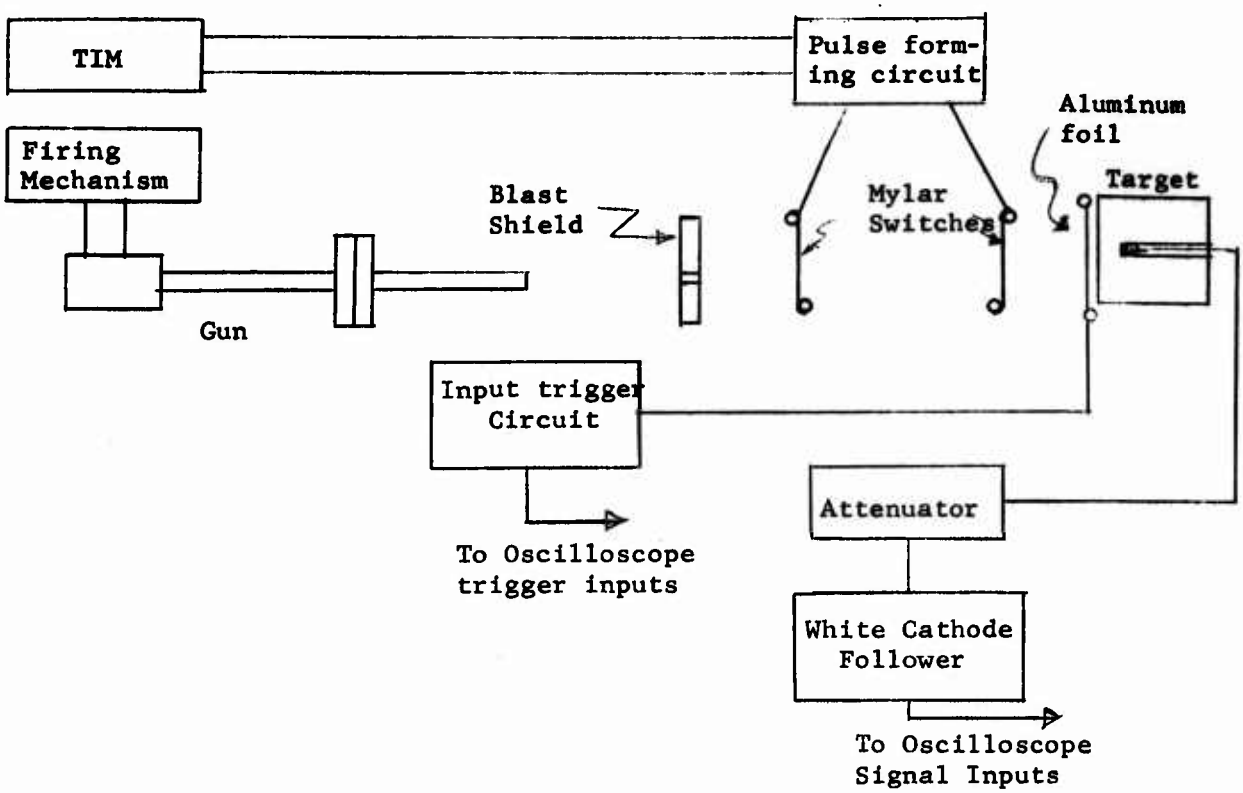

Fig. 17. Sketch of complete experimental system.

firing was done in the concrete lined tunnels of the laboratory and controlled from a position outside of the tunnel.

A series of tests was conducted to determine the mass loss of projectiles used in the experiment. Firings into wax and recovery of projectile fragments indicated a loss of less than 1% for the highest velocities.

4. EXPERIMENTAL RESULTS

The data from any one test were obtained by simultaneously viewing the voltage output of the experimental system on three different oscilloscopes at various time scales, i.e., 1.0 μsec/cm, 5 μsec/cm,

20 μsec/cm, etc. The three oscilloscopes were also assigned different amplitude factors, i.e., 0.05 v/cm, 0.1 v/cm, 0.1 v/cm. The greatest sensitivity being assigned to the fastest sweep time. This would be the 1.0 μsec/cm time scale in the above group of settings. The oscilloscope trace records were made on Polaroid Film.

The oscilloscope trace records were analyzed by using an opaque projector. The pictures were enlarged by this means, so that the distance between the 1 centimeter marks on the film was measured to be 10 centimeters. This proved to be quite a satisfactory -- though very tedious -- method of obtaining accurate data.

Fig. 18 shows the oscilloscope trace of a typical shot. Impact occurred directly over the transducer, which was located 5.576 mm. below the surface.

The question of whether or not there was any significant reflection of the stress pulse at the aluminum-amalgam interface was considered using Eqs. 9, 10, and 11. It was determined that this particular aspect of the problem would be of little consequence, in view of the relative values of the acoustic impedance of the two materials.

The measured value of the logarithmic decrement was used to calculate the losses due to internal friction (16, p. 321) which is strain-amplitude dependent and frequency-independent. This was done for a stress pulse transmitted through the amalgam. There was no significant loss due to internal friction.

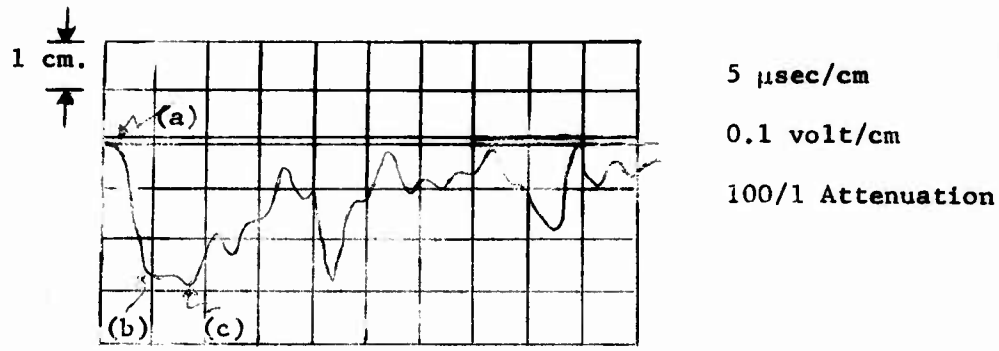

Fig. 18. Oscilloscope trace of transducer output for an impact velocity of 0.091 Km/sec. (Indicated points are discussed in the text.)

4.1 Time Measurements

The time measurement of prime importance is that denoted by point (a) in Fig. 18. This is the time of arrival of a disturbance at the position of the transducer.

A total of 27 targets was used in this experiment. Each target was impacted at least twice (some, as many as six times), once with a low-velocity projectile approximately 0.1 Km/sec, and once at a high velocity of approximately 1.0 Km/sec. Some targets were hit with projectiles with a high velocity of approximately 2.0 Km/sec.

The data obtained from the first ten targets were corrected as follows; it was assumed that a compressional wave could precede the projectile, cause the aluminum foil to contact the target prior to actual contact, thereby giving a late time, since the oscilloscope had been triggered early. The paper used to separate the foil from the target was found to be 0.005 in. thick. Thus a correction factor was obtained by using this distance and the velocity of the projectile for a particular

shot. The time measurements are tabulated in Appendix V.

The distances given in the table are measured from the front or impact surface in the case of the aluminum. The values given for the amalgam are simply the thickness of the amalgam. These distance figures are corrected for the cases where the impact was not directly over the position of the transducer. Several of the targets were cut open or sectioned through the position of the transducer and any discrepancies in the measurements were used to correct the data in the table.

The table contains a "calculated time" for the arrival of the first disturbance at the position of the crystal. This value was obtained by simple calculation using the sonic velocities for the aluminum and amalgam reported in Section 3.2 and Section 3.5.

Figure 19 is a plot of the experimentally determined time of arrival of the disturbance or stress pulse at the transducer vs. the "calculated time" noted above. The solid line represents the ideal case. The dashed line is the location of the least squares fit to the experimental data.

The sonic velocities used for this analysis were obtained from experimental measurements with the composite oscillator. (See Appendix I).

Figure 20, is a plot, similar to that of Fig. 19, with the exception that the sonic velocity for the aluminum "calculated time" is taken from the American Institute of Physics Handbook.

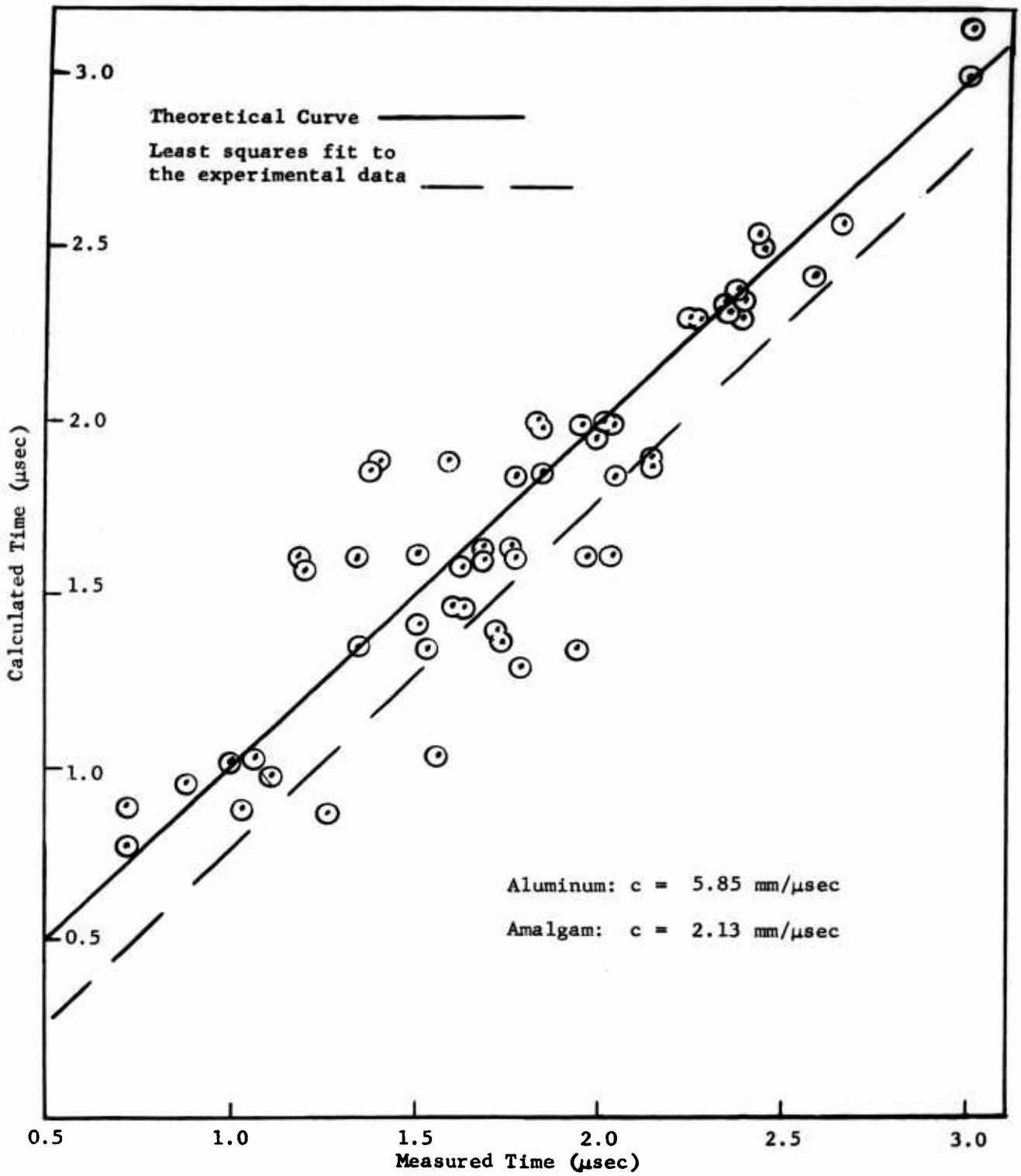

Fig. 19. Calculated time vs. measured time for time of arrival of stress, using measured values of sonic velocity.

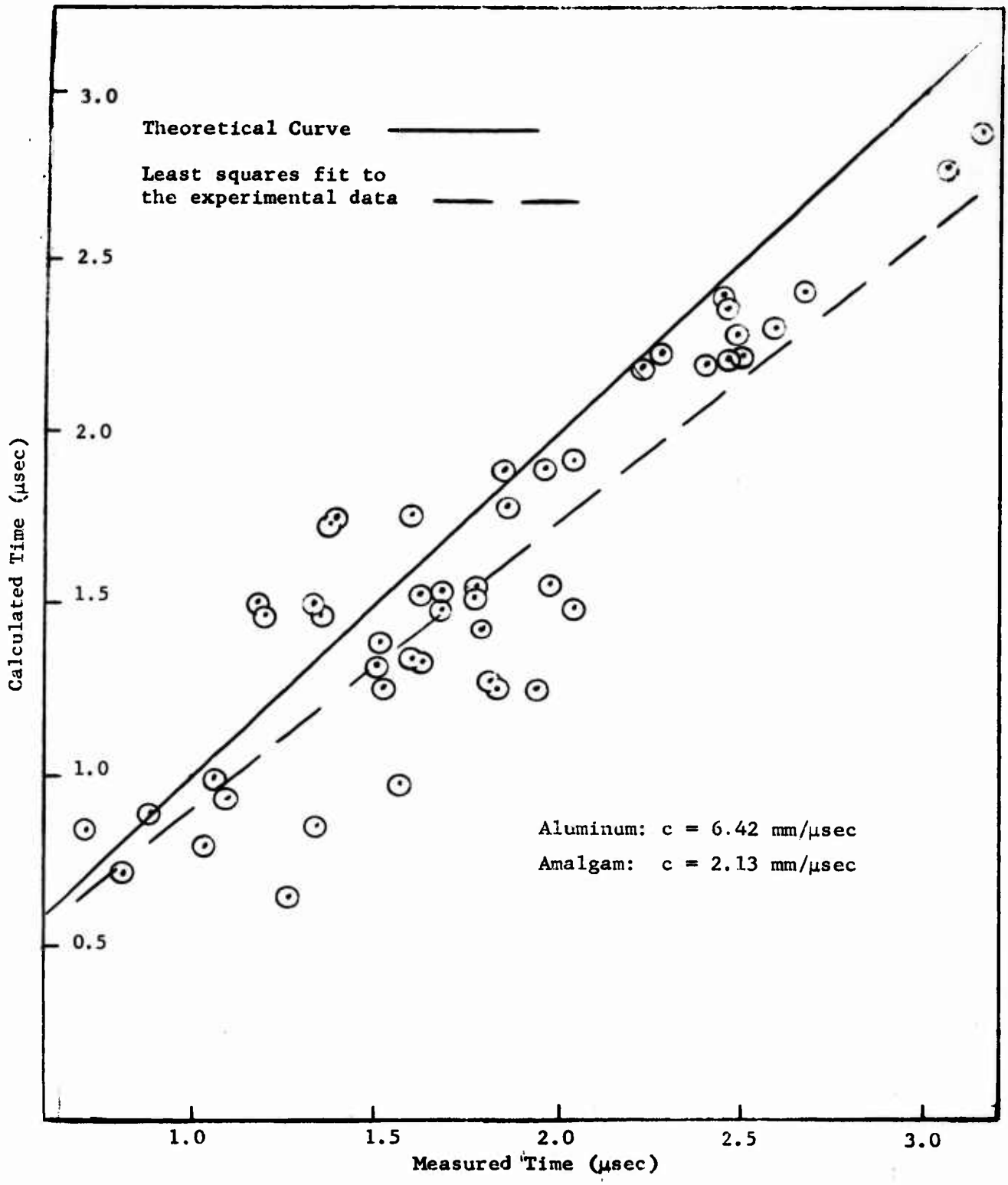

Fig. 20. Calculated time vs. measured time for time of arrival of stress, using A.I.P. Handbook value for aluminum sonic velocity.

4.2. Stress Measurements

A comparison of the pulse shape shown in Fig. 18, with that of Fig. 5(b) discloses a unique identity of form. (Note: Both the amplitude polarity and direction of time axes are reversed in the two figures, one from the other.) The assumption was made that this particular pulse shape actually did represent a double wave in which the peak at point (b) is the elastic wave maximum stress, and that the peak at point (c) is the plastic wave maximum stress. All the pictures were examined for evidence of this double wave character. A limited number was found to have rather definite indications. The voltage amplitudes for each peak were taken from these promising photographs. These voltage data were converted to a stress level, using the constant reported in Section 3.1, which is 25×10^{-5} (Volts/m)/(Newton/m^2).

The point of impact is assumed to be essentially a point or spherical source, and thus the pressure or stress would propagate as described in Eq. 6 with a dependence on 1/r. Further, if a plastic wave or pulse is propagating through the material, one might expect it to attenuate in some manner -- perhaps exponentially. Thus a generalize stress pulse might be described as:

$$\sigma = \frac{C}{r} e^{-\alpha r} \qquad (12)$$

where σ is the stress, C is a constant, r is the radial distance from the source, and α is an attenuation constant. We note that if the wave is elastic in character the attenuation constant will be zero.

The above equation is multiplied by the factor r, and then the logarithm is taken, the equation then becomes

$$\log(\sigma r) = -\alpha r + \log C \qquad (13)$$

The stress data obtained from the photographs which indicated a double wave structure are plotted on a semi-log plot as shown in Fig. 21. The data for the first peak are indicated by the circles and that for the second peak by the squares. The points plotted in Fig. 21 are for a restricted impact momentum range. It is to be expected that the stress level initiated in the target will depend upon the impact parameters of the projectile in some manner. These tests were conducted in such a manner as to control the velocity of the projectile as nearly as possible to particular chosen values; i.e., 0.1 Km/sec and 1.0 Km/sec.

4.3 Transducer Break-up

Examination of the targets after completion of the impact tests disclosed two cases in which the crater had penetrated through to the transducer. The signal output of the transducer in this case could possibly indicate that this had happened. This would then give more information concerning the actual cratering process. The oscilloscope trace for one of these two cases is shown in Fig. 22. The projectile hit approximately 1 mm. off-center. The transducer is located 5.28 mm from the impact surface.

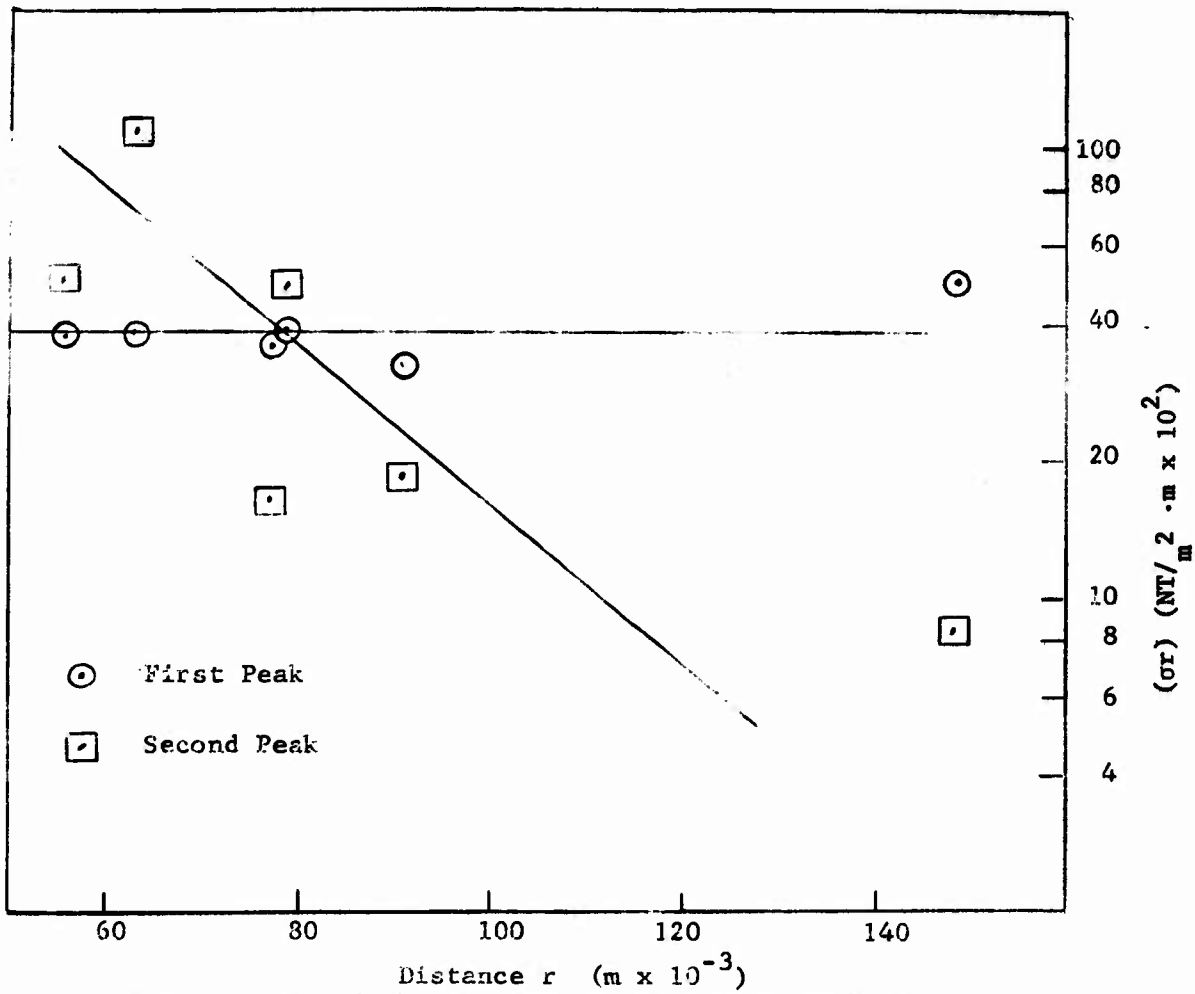

Fig. 21. Log (σr) vs. r for two-wave structure of transducer output signal--low momentum range.

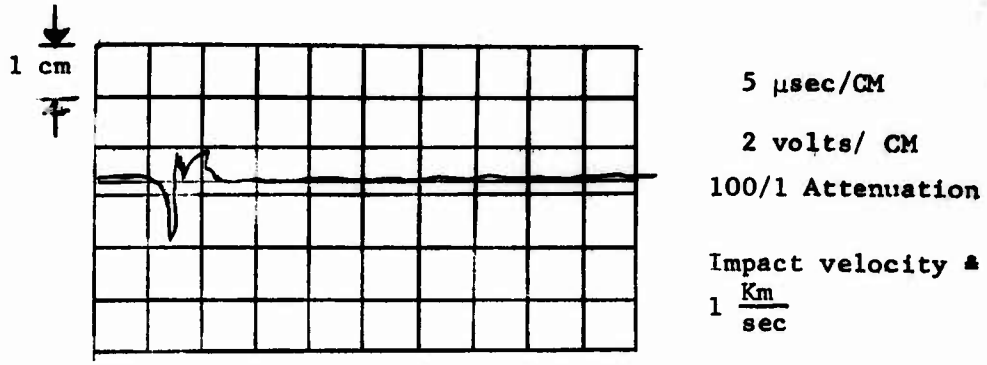

Fig. 22. Oscilloscope trace indicating possible transducer breakup.

5. DISCUSSION

5.1. Time Measurements

The plot of the corrected experimental time vs. the "calculated time" shown in Fig. 19 indicates the degree of success of the experimental arrangement, when elastic theory is used as a basis for comparison. The slope of the least-squares-fit straight line is 1.030, with an intercept on the vertical axis of -0.131 μsec. The standard deviation was found to be 0.249. An effort was made to determine the reason for spread in the data. This did not prove successful, beyond the corrections noted previously. The value for the slope of the least squares line is remarkably close to the theoretical value of 1.00. The sonic velocity used to make this plot is that obtained by measurement with the composite oscillator. The same experiment was used to obtain the sonic velocity for the amalgam.

This same type of plot is shown in Fig. 20; however, the "Handbook"

value for the aluminum sonic velocity is used in this case.[20] Here the slope of the least-squares-fit straight line is 0.885, with a vertical intercept of ∮0.058. The standard deviation was found to be 0.233.

5.2. Stress Measurements

It was noted above in Section 4.2, that if the wave is elastic in character the attenuation constant α in Eq. 12 or 13 would be zero. It is significant that the plot of the points for the low momentum range and for the first (elastic) peak, as indicated by the photographs, fits a straight line with zero slope. It is also significant that the plot of the points for the second (plastic) peak shows a greater scatter and a definite trend which is indicated by the straight line of negative slope. See Fig. 21.

It should be recalled that the output characteristic used to determine the stress level from the voltage measurements for this plot is an average value of transducers which were not used in the targets. Thus, individual variation from one transducer to the other may cause a variation in the stress level by a factor of from 2 to 5. It was not possible to attain exactly the same projectile velocity from one shot to another. Thus it was necessary to choose a "range" of momentum. This would have an effect on the scatter of the points in Fig. 21.

It is also noted that there is a small number of points used in this analysis. This was primarily due to the pioneering nature of the experimental work. It is felt that these experimental limitations only serve

to heighten the significance of the plot in Fig. 21.

This same analysis was tried for two cases of higher momentum range. It did not prove successful, primarily because of the lack of sufficent data points; that is, there were very few double-wave type oscilloscope traces for the higher momentum ranges.

5.3. Experimental Technique

Several of the targets were cut open or sectioned through the crater and hole for mounting the transducer. This procedure disclosed a few errors in the initial measurements of hole dimensions. However, the major observation was that the technique for mounting the transducers proved to be quite satisfactory. There were many examples where the amalgam and/or the transducer remained in position in spite of the tearing action of the saw used to section the target. One of the targets in which the epoxy bonding agent was used to mount the transducer was sectioned. This clearly demonstrated the superiority of this method of mounting. The crystal was found to be in very close contact with the bottom of the hole, with the remaining portion of the hole filled with the epoxy. The action of the saw did not pull or tear the crystal or the epoxy. The sectioning of the targets also demonstrated that the cratering process is not disturbed by the removal of target material to mount the transducer. The classical crater shape was obtained in each case, even in the case where the crater depth was such that the wall between the hole and crater was nonexistent.

6. CONCLUSIONS

The evidence which is graphically displayed in Fig. 19, shows that the experimental procedure for making the time measurements associated with stress pulses in a target under high velocity impact is satisfactory. The differences between the graphs of Fig. 19 and Fig. 20 demonstrate that this method could be used successfully to measure sonic (elastic) wave velocities, since the two figures are essentially a comparison of experimental work with handbook values.

It was found possible to identify a double wave that can be associated with elastic and plastic phenomena occuring during the cratering process, or impact process for low momentum projectiles. The identification of the double-wave pulse shapes is confirmed by the evidence of Fig. 21; that is, the first peak stress, as identified from the photograph, shows no attenuation. The points associated with the second peak stress show a very definite trend, as indicated by the straight line, and the slope of this indicator line is negative as predicted.

The question as to whether it is possible to determine when the transducer breaks up and correlate this with the crater depth is inconclusive for lack of sufficient data.

The experimental technique has proven to be quite satisfactory as a means to study stress pulses initiated in solid targets by high-velocity projectiles. This is indicated by the evidence noted above concerning the sectioned targets, in addition to the successful analysis of the data obtained from the transducers themselves.

The calibration experiments demonstrated that the output of the transducer can be closely correlated with that of suitably mounted "coincident" strain gages.

Further application of the system developed in this research should provide more satisfactory information about the intricate, but still largely unknown processes which attend the formation of craters in semi-infinite targets.

APPENDIX I

THE COMPOSITE OSCILLATOR

The composite oscillator is widely used as a method to measure the internal friction of materials. It is a piezoelectric 3-component oscillator. The assembly used consists of two X-cut matched quartz bars of 1/8 inch square cross section driven in longitudinal oscillation at or very near 50 kilocycles. The specimen to be studied is mounted on these two bars and is progressively cut to resonate at the same fundamental frequency. Silver electrodes are plated on two opposing sides of the quartz bars and serve to drive the system in resonance, and to measure the amplitude of the oscillation at the same time. The system is analyzed in detail by Marx.[23]

The maximum displacement and strain amplitude present in the composite oscillator assembly at its fundamental resonance is shown in Fig. 23.

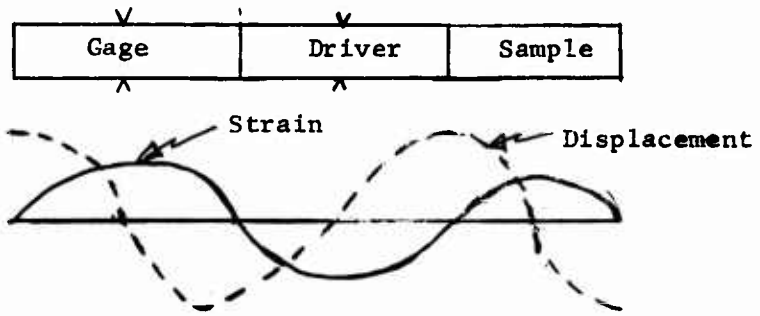

Fig. 23. Vibrational and displacement amplitude limits for the composite oscillator.

The quartz crystals labeled gage and driver are supported at displacement nodes. When the system is in fundmental or odd-harmonic longitudinal vibration, the support losses are minimized and energy losses are ascribed to other processes.

For a given specimen the strain amplitude can be written as

$$\epsilon = BV_g \tag{14}$$

where the constant B is calculated using measured circuit parameters, and V_g is the voltage measured at resonance on the gauge crystal.

The damping for a given specimen is expressed as

$$\delta_t = A(V_d/V_g) \tag{15}$$

where V_d is the voltage applied to the driver crystal, V_g is the same as noted above, and the constant A must be determined from physical and circuit parameters.

Samples of the target material and of the amalgam were prepared and mounted on this oscillator. When the proper length for resonance has been obtained, this information is conjunction with the exact frequency of resonance can be used to determine the sonic velocity in the sample. That is, its length will be exactly one-half wavelength. It should be noted that this is longitudinal vibration of a rod. Thus it is the longitudinal rod sound velocity that is determined in this manner.

Dr. M. H. Miles of the Solid-State Physics Laboratory constructed a

different type of composite oscillator. It operates on the same general principles, but the oscillator vibrates in a torsion mode. Samples of both the aluminum target material and the amalgam were tested on this torsion oscillator. A simple analysis of the resonant frequency and the resonant length of the sample then allows the determination of the shear wave sonic velocity in the sample.

We refer to Eqs. 2, 3, 4 in Section 2.1 and note that in order to determine the longitudinal (dilatational) velocity for a given material one must have values for the bulk modulus of elasticity, and the shear modulus. The shear sonic velocity is dependent upon the shear modulus as shown in Eq. 3, and the longitudinal rod sonic velocity is dependent upon the Young's modulus as indicated by Eq. 4. Thus if one obtains from these relationships the two moduli -- and this can be done, since the sonic velocities are known -- it is possible to use these two values to calculate the bulk modulus of the material, and from there make use of Eq. 2 to determine the longitudinal velocity of sound for the material tested.

In order to test the output of the transducer while mounted on the oscillator, it was necessary to make up a composite sample. It was noted that the length of the sample is critical, in order that the oscillator can vibrate in resonance. The transducers themselves are far too small for this condition, thus the arrangement shown in Fig. 24 was used to make these tests.

It was necessary to make the assumption that the distribution of

different type of composite oscillator. It operates on the same general principles, but the oscillator vibrates in a torsion mode. Samples of both the aluminum target material and the amalgam were tested on this torsion oscillator. A simple analysis of the resonant frequency and the resonant length of the sample then allows the determination of the shear wave sonic velocity in the sample.

We refer to Eqs. 2, 3, 4 in Section 2.1 and note that in order to determine the longitudinal (dilatational) velocity for a given material one must have values for the bulk modulus of elasticity, and the shear modulus. The shear sonic velocity is dependent upon the shear modulus as shown in Eq. 3, and the longitudinal rod sonic velocity is dependent upon the Young's modulus as indicated by Eq. 4. Thus if one obtains from these relationships the two moduli -- and this can be done, since the sonic velocities are known -- it is possible to use these two values to calculate the bulk modulus of the material, and from there make use of Eq. 2 to determine the longitudinal velocity of sound for the material tested.

In order to test the output of the transducer while mounted on the oscillator, it was necessary to make up a composite sample. It was noted that the length of the sample is critical, in order that the oscillator can vibrate in resonance. The transducers themselves are far too small for this condition, thus the arrangement shown in Fig. 24 was used to make these tests.

It was necessary to make the assumption that the distribution of

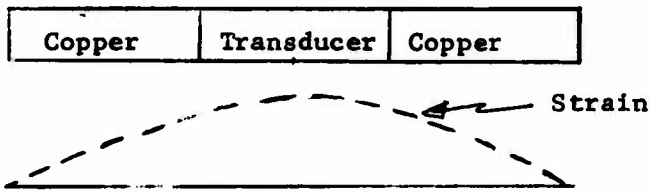

Fig. 24. Composite smaple for testing of barium titanate transducer in the composite oscillator.

strain amplitude is essentially as indicated in Fig. 24. That is, the copper-transducer boundary did not sensibly alter the strain distribution throughout the composite sample when compared with that of a uniform, single material sample.

The composite sample was placed in the longitudinally vibrating oscillator. The output of the crystal or transducer was displayed on an oscilloscope. At the fundamental resonance frequency of the assembly, there was a dramatic change in the output of the transducer. The output was measured from the oscilloscope trace, and the gage voltage V_g, was measured. This information allows one to obtain a relationship between a given strain amplitude and the voltage output of the transducer. The results of this determination agree very closely with those obtained from the semi-static and the rod-to-rod impact tests.

APPENDIX II

SOME PROPERTIES OF BARIUM TITANATE

The following will be a discussion of some of the salient features which distinguish barium titanate ceramic from ordinary piezoelectric materials. Barium titanate is commonly called ferroelectric, which for all practical purposes means that an untreated piece of the material will exhibit a strain which is proportional to the square of the electric field strength.[16]

The crystal structure of barium titanate is shown in Fig. 25.

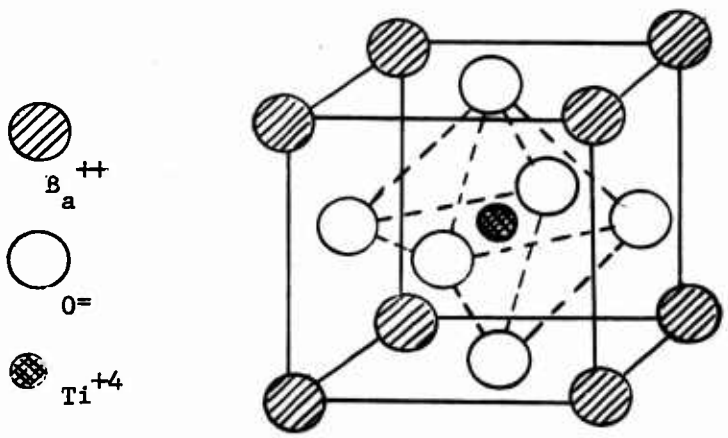

Fig. 25. Crystal structure of barium titanate.

The titanium atom is taken as the center of symmetry. It is easily displaced by an electric field because of its small size relative to the surrounding ions. The barium titanate is found to change from a tetragonal to cubic structure if the temperature is raised above the Curie point of the material. In the tetragonal phase, the titanium

atom tends to move toward one of the face-centered oxygen atoms. Each crystal cell, therefore, has a dipole moment which may be oriented toward any one of the six oxygen atoms. Since the orientation of the dipole moment within one cell is influenced by the orientations in neighboring cells, there are regions of parallel alignment, called "domains."

If a strong electric field is applied, the electric axes of the domains oriented at right angle to the field are turned into the direction of the field and uniaxial crystal is created in which all the tetragonal phase c axes are parallel to the field. If the field is reversed, the c axes will eventually switch around 180°.

If a strong d-c field is once applied, some of the induced domain alignment persists. In fact, when a barium titanate material has three or four per cent of lead in the form of lead titanate mixed with it and this mixed ceramic is polarized at a high field strength at temperatures above the Curie temperature, then cooled under the applied field, the remanent polarization could not be removed by any reversed field that could be applied up to a temperature of 70° C.[18] This remanent polarization renders the material piezoelectric in character.

When a permanently polarized piece of barium titanate is raised in temperature above its Curie temperature, it loses its piezoelectric character and once again becomes ferroelectric.

In general, a piezoelectric material will produce charges by straining the material in the direction of the polarization. The charge

developed per unit cross-sectional area; i.e., the polarization is given by

$$P_i = e_{ik}\, x_k = Q/S \tag{16}$$

in which $x_k = \Delta\ell/\ell$ is the strain, and e_{ik} represents the piezoelectric stress constant. The subscripts refer to crystal directions. This same material, with conducting electrodes on one pair of faces behaves like an electric capacitor described by the familiar equation:

$$C = \epsilon\, \epsilon_o \frac{S}{l} = \frac{Q}{V} \tag{17}$$

At the same time this piece of material behaves like a mechanical spring, the stiffness constant c_{hk} is given by Hooke's Law

$$c_{hk} = (F/S)/(\Delta\ell/\ell) \tag{18}$$

where again, the subscripts allow for crystal anisotropy.

A simple algebraic manipulation of these three equations will then lead to the following expression:

$$V = \left[e_{ik}(F/S)\ \ell\right] \Big/ \left[\epsilon\, \epsilon_o\, c_{hk}\right] \tag{19}$$

Thus we see that the voltage produced between the two electrode faces of piezoelectric material is directly proportional to the force (or the stress) applied to those electrode faces.

Measurements were made on three different transducers as outlined in Section 3.9, Item 3, Semi-static Measurements. An average value was taken in each case. The results were:

Transducer No.	(Volts/m)/(Newton/m^2)
12	15.7×10^{-5}
19	26.3×10^{-5}
24	35.8×10^{-5}
37*	25.6×10^{-5}
23**	21.0×10^{-5}

* Measurement from rod impact test -- average value.

** Measurement from composite oscillator tests -- average value.

APPENDIX III

TRANSDUCER TESTING

A schematic diagram of the test apparatus used to measure the first mechanical resonance of the barium transducers is shown below in Fig. 26.

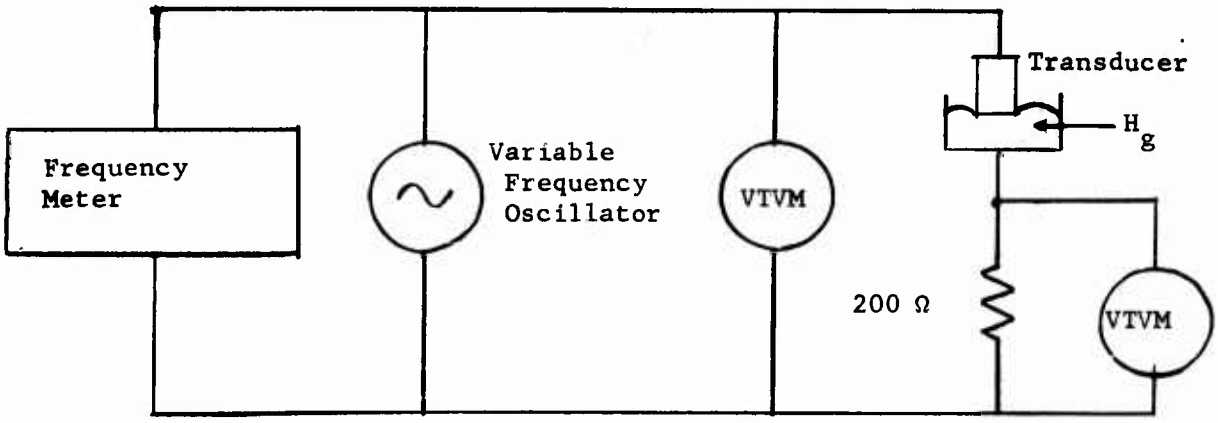

Fig. 26. Schematic diagram for resonance test of transducers.

The transducer was arranged in such a manner that it just barely touched a "bath" of liquid mercury with minimum mechanical restraint. A constant input voltage of 5 volts was applied to the unit. The frequency of the applied voltage was varied from 1,000 cps to 500,000 cps. The voltage across the 200 ohm resistance in series with the transducer was measured in order to detect this resonance. Resonance was indicated by a very rapid increase in this latter voltage.

The Berkeley Universal Counter, Model 7360, was used as a "frequency meter."

APPENDIX IV

ELECTRONIC CIRCUITS

Capacitor Compensated Resistor-Divider Network

As noted in the body of this thesis (page 30), it was found necessary to attenuate the signal obtained from the transducer. It was thought desirable to obtain this attenuation without degrading the rise-time of the signal. This can be achieved through the use of the circuits shown in Fig. 27.

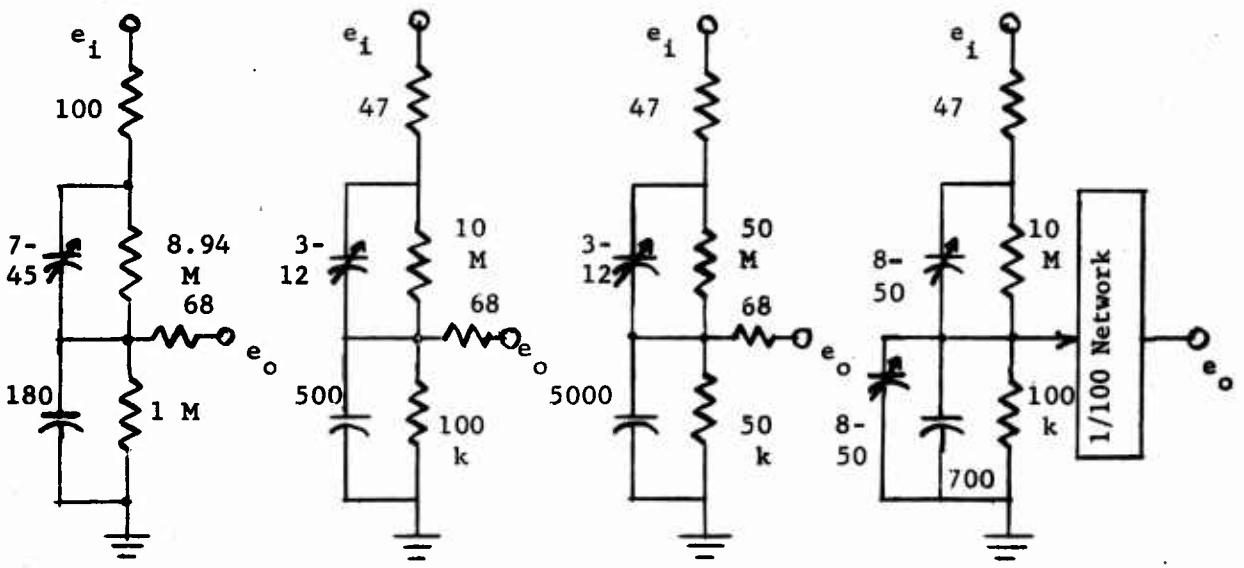

All capacitors in picofarads
All resistors in ohms

Fig. 27. Capacitor compensated resistor-divider networks.

The output signal of such networks will not be altered if the time constants (RC) of the two branches are equal.[26] The voltage transfer function becomes $e_o/e_i = R_2/(R_1 + R_2)$.

The resistors are 1% Deposited Carbon in order to reduce the inductive effects to a minimum. Incidentally, this will also improve the accuracy of the network.

Silvered-mica capacitors were used wherever possible since they have the best tolerances (5%) and the best performance in pulse networks. The dielectric of ceramic capacitors requires a certain finite time to polarize upon application of a voltage. In pulse work this time has an appreciable effect on the operation of the capacitors. This results in the introduction of extraneous effects, such as degrading the rise-time, noise, etc.

Standard ceramic trimmer capacitors are used where indicated. They are used to obtain the final values necessary to "tune" the network according to the above condition.

The tuning is performed with the standard square-wave testing procedure. The square-wave is fed into the attenuator network and the output displayed on an oscilloscope. The trimmers are then adjusted until the attenuated square-wave has a true square-wave character without either overshoot or undershoot of the leading edge.

The attenuator is built on a phenolic board to reduce the possibility of noise pick-up.

The small 47 ohm and 68 ohm, and in one case 100 ohm, series input and output resistors were added to the attenuator circuit in order to cut out ringing in the circuit and also to eliminate effects of reflections on the various coaxial cables.

Note, one should exercise some care to make sure that the capacitors have the proper voltage ratings for the voltage pulses which are expected as output signals from the transducer.

The resistors are 1% Deposited Carbon in order to reduce the inductive effects to a minimum. Incidentally, this will also improve the accuracy of the network.

Silvered-mica capacitors were used wherever possible since they have the best tolerances (5%) and the best performance in pulse networks. The dielectric of ceramic capacitors requires a certain finite time to polarize upon application of a voltage. In pulse work this time has an appreciable effect on the operation of the capacitors. This results in the introduction of extraneous effects, such as degrading the rise-time, noise, etc.

Standard ceramic trimmer capacitors are used where indicated. They are used to obtain the final values necessary to "tune" the network according to the above condition.

The tuning is performed with the standard square-wave testing procedure. The square-wave is fed into the attenuator network and the output displayed on an oscilloscope. The trimmers are then adjusted until the attenuated square-wave has a true square-wave character without either overshoot or undershoot of the leading edge.

The attenuator is built on a phenolic board to reduce the possibility of noise pick-up.

The small 47 ohm and 68 ohm, and in one case 100 ohm, series input and output resistors were added to the attenuator circuit in order to cut out ringing in the circuit and also to eliminate effects of reflections on the various coaxial cables.

Note, one should exercise some care to make sure that the capacitors have the proper voltage ratings for the voltage pulses which are expected as output signals from the transducer.

White Cathode Follower

The well-known conventional cathode follower has been analyzed thoroughly in the literature.[30] It will function as an impedance transformer from high input impedance to low output impedance. However, it posses certain inherent limitations in transient response and output impedance. With large tube currents, the "operating point" of the tube is changed and non-linear operation results. Further, the conventional cathode follower will not handle signals of either polarity equally well.

The White cathode follower bears the name of E. L. C. White who patented it in 1944.[31] It is a two-tube series device that can provide output impedances of the order of 5 ohms and transmits pulses of either polarity with minimal distortion.[27,32,33]

The circuit used in these experiments is shown in Fig. 29. It has been modified somewhat to fit our particular needs.

The ECC/88 or 6DJ8 tube was chosen bacause of its high value of transconductances and because it is a double triode in a single envelope with a screen between the two triodes which can be used to shield one tube from the other. The pin connections are shown in Fig. 28.

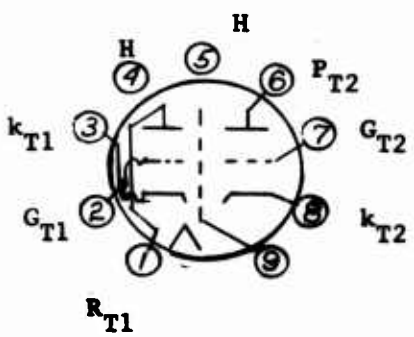

Fig. 28. Pin connections for ECC/88 or 6DJ8 electron tube.

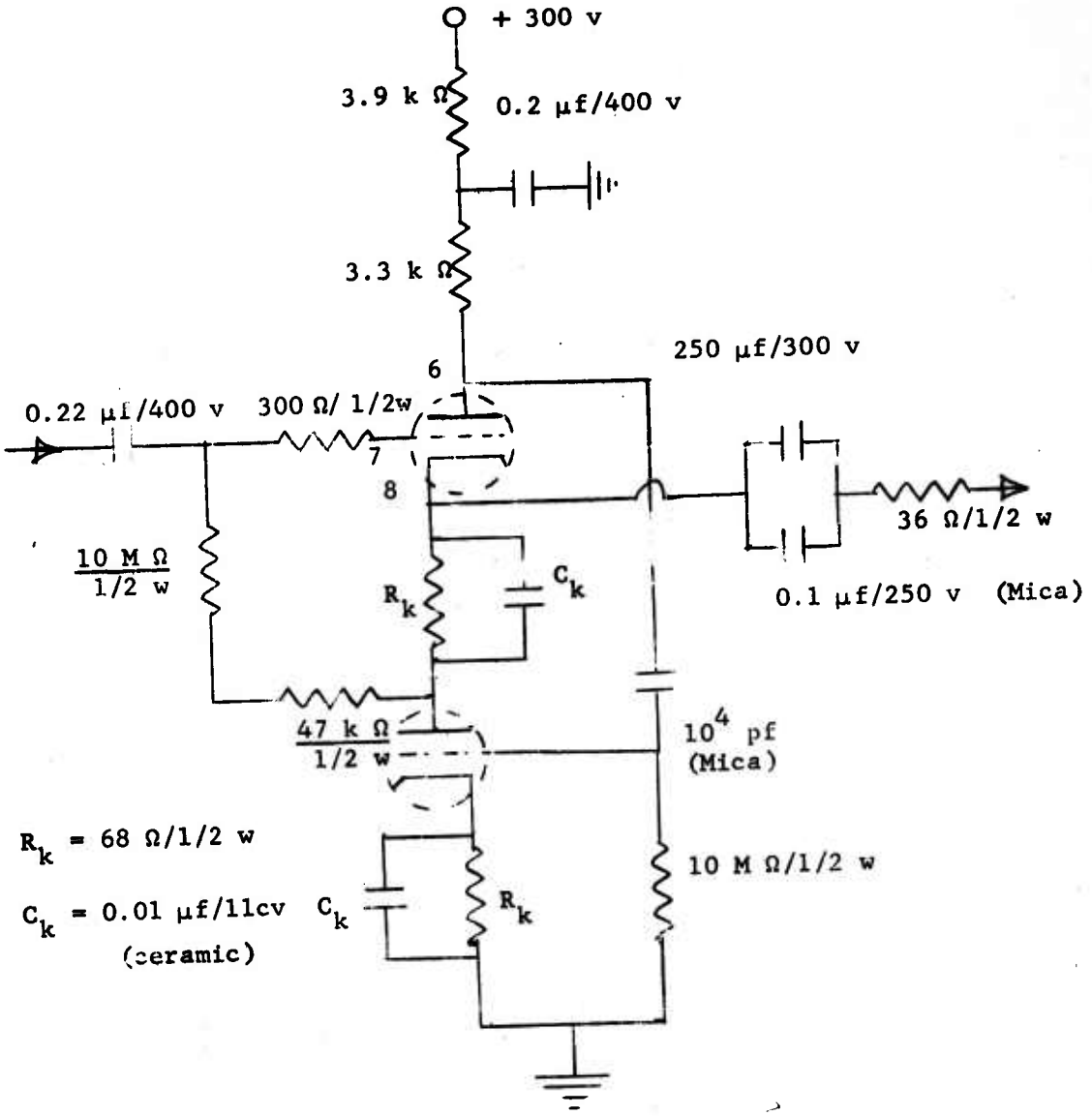

Fig. 29. Modified White cathode follower.

Certain items of interest should be pointed out. The circuit, along with its power supply and voltage regulator, is mounted on phenolic board. The leads are kept as short as possible. These precautions reduce stray capacitance and inductive effects. The output-coupling capacitor, actually two capacitors, is a parallel combination of 0.1 μf (mica) and a 250 μf (electrolytic). The first capacitor is to take care of the high frequencies and the second is to handle the lower frequencies. This gave the circuit better characteristics as far as "sag" is concerned. The 36 ohm series output resistor was inserted by trial and error to reduce the reflections apparent in the output signal. It also assisted in the attainment of the desired attenuation ratios.

When examining the White cathode follower by itself, it is necessary to use an input L-pad of resistance as shown in Fig. 30. This must be

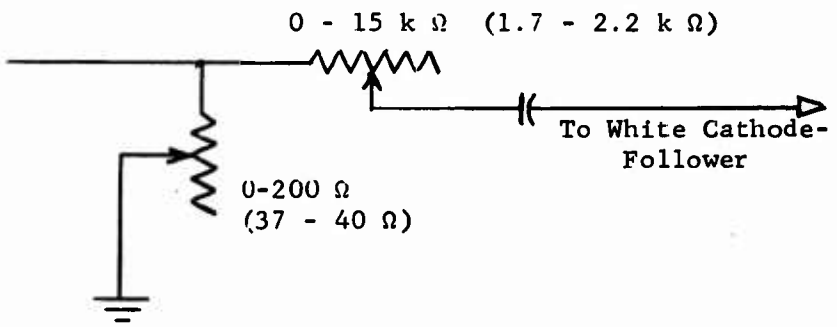

Fig. 30. Input L-pad used to examine White cathode follower.

removed when the attenuator is coupled to the White cathode follower. The values in the brackets represent the approximate optimum values set into the variable resistance.

The Power Supply used for this circuit is a packaged plug-in unit--

octal plug.[34] The Voltage Regulator used in the circuit is shown in Fig. 31.

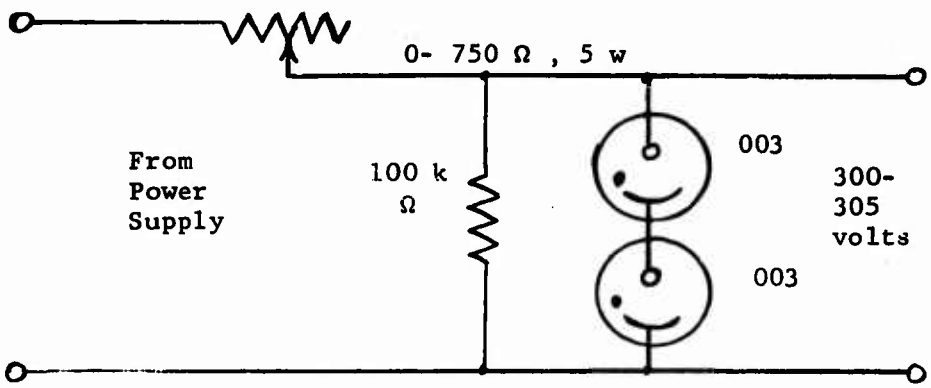

Fig. 31. Voltage Regulator

The White cathode follower has a gain very nearly equal to 1.0. The sag is approximately 5% at a frequency of 100 kc when observing a square wave of this frequency. The rise time (10% - 90%) of the attenuator and White cathode follower system was measured and found to be 0.03 μsec to 0.05 μsec. The time delay of the signal in passing through this system was measured and found to be 0.08 μsec to 0.09 μsec.

The following are the design equations used in the design of the circuit. The schematic circuit with its symbols is shown below along

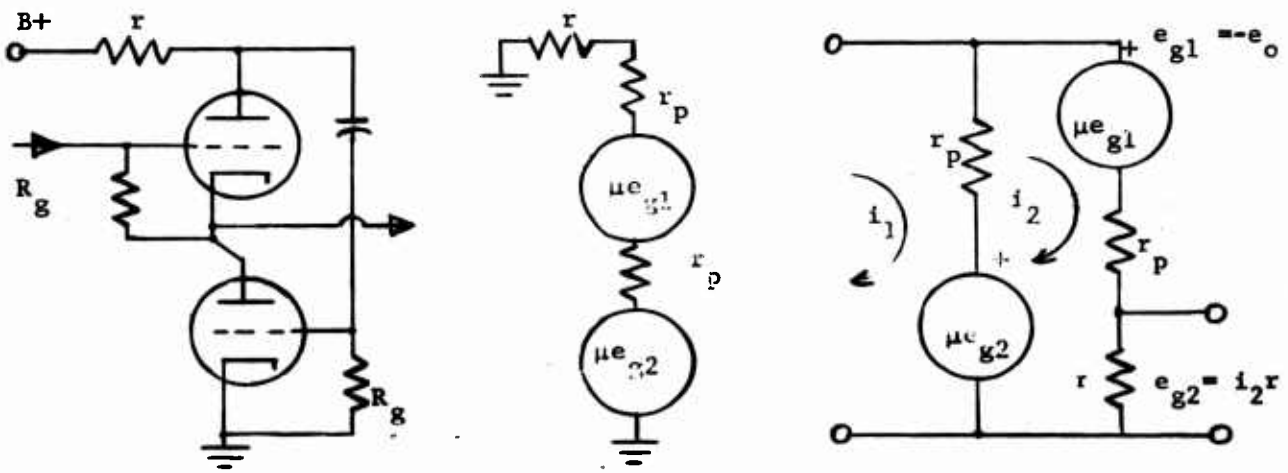

Fig. 32. Circuits used for White cathode-follower design.

with the equivalent circuit used to calculate the output impedance (for no input).

The equations are:

$$e_o - (i_1 - i_2)r_p + \mu e_{g2} = 0$$

$$-\mu e_{g1} - i_2(r_p + r) - \mu e_{g2} - (i_2 - i_1)r_p = 0$$

These equations reduce to:

$$R_{out} = \frac{r_p(r_p - r)}{[r_p(\mu + 2) + r(1 + \mu + \mu^2)]} \qquad A = \frac{2\mu^2 R_L}{2R_L(\mu^2 + \mu + 1) + r_p(\mu + 1)}$$

$$r = \frac{1}{g_m} + \frac{2R_L}{\mu}$$

The gain equation is obtained from Pulse and Digital Circuits by Millman and Taub, pp. 99-101, and p. 620, McGraw-Hill.

APPENDIX V

Experimental Data

Time Measurement Data

See Fig. 33, for distances.

Target No.	Shot No.	Velocity	d_1* (Al.)	d_2* (Am.)	Calculated** Time	Measured Time
		Km/sec	mm.	mm.	μsec	μsec
1	1	0.099	5.56	1.91	1.85	1.77
	2	0.135	5.67	1.95	1.89	2.14
	3	0.151	5.56	1.91	1.85	2.04
	4					no time
	5	0.440	5.56	1.91	1.85	1.83
2	2	0.107	5.69	2.08	1.95	1.97
3	1	0.100	8.84	2.18	1.99	1.83
	2	0.100	5.64	2.22	2.01	2.02
	4	2.038	5.64	2.18	1.99	1.94
4	1	0.112	6.90	1.74	2.00	1.82
6	1	0.100	7.45	2.28	2.35	2.26
	2	0.159	7.33	2.25	2.31	2.45
	3	1.00	7.91	2.42	2.49	2.44
7	3	0.178	6.97	2.60	2.42	2.57
	4	1.188	6.90	2.57	2.39	2.36
8	1	0.103	9.08	2.10	2.54	2.43
	3	1.155	9.14	2.12	2.56	2.65
9	1	0.083	7.61	2.13	2.31	2.22
	2	0.180	7.60	2.13	2.30	2.38
	3	1.203	7.76	2.17	2.34	2.48

Target No.	Shot No.	Velocity	d_1* (Al.)	d_2* (Am.)	Calculated** Time	Measured Time
10	1	0.108	6.01	1.30	1.64	1.76
	2	0.106	5.91	1.28	1.61	1.76
	3	0.117	6.01	1.30	1.64	1.67
11	4	0.118	3.55	0.929	1.04	1.06
	5	0.181	3.79	0.805	1.03	1.33
14	1	0.092	6.87	0.847	1.57	1.19
	2	0.175	7.04	0.868	1.61	1.33
	3	1.173	7.04	0.868	1.61	1.17
15	1	0.108	8.10	1.02	1.86	1.37
	2	0.183	8.21	1.03	1.89	1.58
	3	1.145	8.15	1.03	1.88	1.38
16	1	0.104	3.88	1.96	1.58	1.61
	2	1.148	3.94	1.99	1.61	1.95
18	1	0.104	13.34	1.52	3.00	3.04
	2	1.095	13.41	1.53	3.01	3.14
19	1	0.107	5.39	0.907	1.35	1.34
	2	1.152	6.09	0.931	1.62	1.67
20	1	0.993	6.43	0.682	1.42	1.50
21	1	0.091	3.88	0.69	0.987	1.10
	2	0.422	4.08	0.726	1.04	1.56
22	1	0.093	5.49	1.46	1.62	1.50
	2	0.877	5.10	1.36	1.51	1.78
24	1	0.086	6.37	0.566	1.35	1.52
	2	0.915	6.37	0.566	1.35	1.90
25	1	0.089	3.32	0.709	0.90	0.71
	2	0.850	3.71	0.525	0.88	1.26
26	2	0.92	12.23	0.392	2.21	1.73

Target No.	Shot No.	Velocity	d_1* (Al)	d_2* (Am.)	Calculated** Time	Measured Time
27	2	0.092	8.20	0.46	1.62	2.03
28***	1	0.0672	5.69	----	0.97	0.875
	2	0.104	4.60	----	0.79	0.810
	3	0.959	5.19	----	0.89	1.03
29***	1	0.108	8.62	----	1.47	1.60
	2	0.108	8.62	----	1.47	1.62
	3	0.102	8.08	----	1.38	1.72
	3.5	0.88	8.18	----	1.40	1.71

* See Fig. 33.

** Using elastic theory and measured values for sonic velocities in aluminum and amalgam.
Velocity of sound in aluminum -- 5.85 mm/μsec (longitudinal)
Velocity of sound in amalgam -- 2.13 mm/μsec (longitudinal)

*** Targets in which transducer is bound in with epoxy.

Stress Measurement Data

Target No.	Shot No.*	d_1/d_2 (r)	Momentum	1st Peak** Amplitude	2nd Peak*** Stress	2nd Peak Amplitude	2nd Peak Stress
		mm.	Kg-m/sec x 10^{-3}	Volts	Newton/m^2 x 10^6	Volts	Newton/m^2 x 10^6
3	1-b	7.82	28	9.5	4.98	12.0	6.33
14	1-b	7.72	23	9.0	4.72	4.5	2.37
19	1-b	6.30	27	12.0	6.30	31.5	17.5
22	1-b	5.58	23	13.0	6.84	17.5	9.21
28	1-b	5.69	17	6.0	3.15	9.0	4.72
15	1-b	9.12	27	6.95	3.65	3.95	2.08
18	1-b	14.86	26	6.5	3.42	1.5	0.80

* The letter following the shot number designates the particular picture.

** See Fig. 18.

*** Using average transducer output coefficient -- 25 x 10^{-5} (Volts/m)/(Newton/m^2)

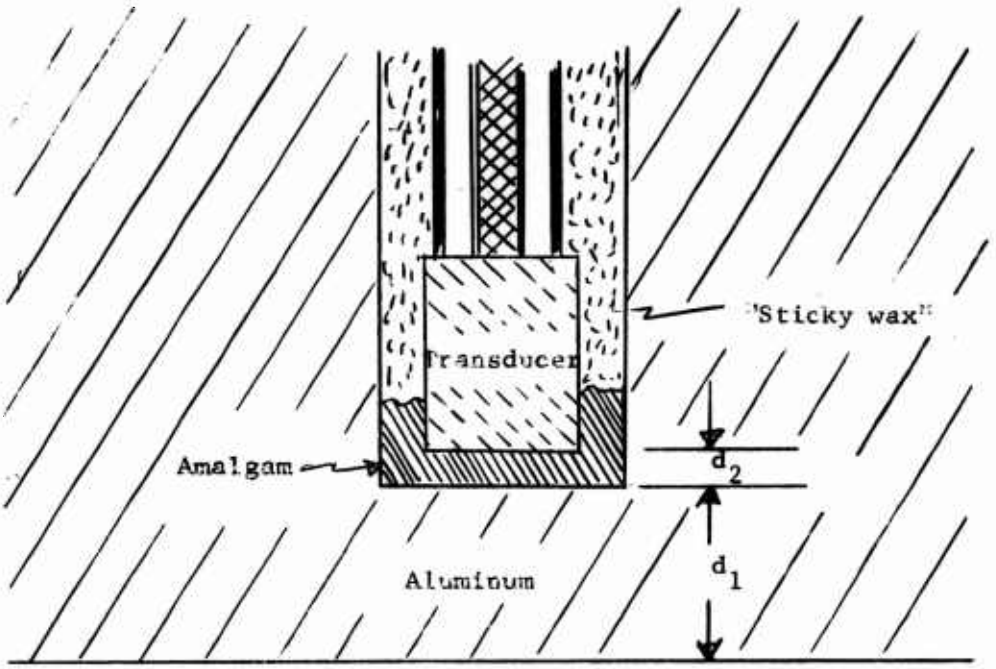

Fig. 33. Idealized schematic cross-section of target and mounted transducer locating distances used in table of data.

REFERENCES

1. W. S. Partridge, H. B. Van Fleet, and C. R. Whited, "Crater Formation in Metallic Targets," Jour. Appl. Physics, Vol. 29, pp. 1332-1336, 1958.

2. W. S. Partridge, and H. B. Van Fleet, "Similarities Between Lunar and High-Velocity Impact Craters," Astrophysical Jour., Vol. 127, 1958.

3. D. K. Johnson, E. T. Cannon, E. P. Palmer, and R. W. Grow, "Cratering Produced in Metals by High-Velocity Impact," Technical Report UU-4 on Contract AF 04(647)-176, High Velocity Laboratory, University of Utah, 1959.

4. G. H. Turner, E. P. Palmer, and R. W. Grow, "Projectile Effects and Subsurface Disturbance in High-Velocity-Impact Cratering in Lead,: Technical Report UU-5 on Contract AF 04(647)-176, High Velocity Laboratory, University of Utah, 1960.

5. Walter Herrmann and Arfon H. Jones, "Survey of Hypervelocity Impact Information," A.S.R.L. Report No. 99-1, Massachusetts Institute of Technology, September 1961.

6. J. M. Walsh, M. H. Rice, R. G. McQueen, and F. L. Yarger, "Shock-Wave Compression of Twenty-seven Metals. Equations of State of Metals," Physical Review, Vol. 108, pp. 196, 1957.

7. L. W. Morland, "The Propagation of Plane Irrotational Waves through an Elastoplastic Medium," Phil. Trans, Roy. Soc., London, Vol. A 251, p. 541, 1959.

8. G. R. Fowles, "Shock Wave Compression of Hardened and Annealed 2024 Aluminum," Jour. Appl. Physics, Vol. 32, p. 1475, 1961.

9. R. L. Bjork, "Effect of Meteoroid Impact on Steel and Aluminum in Space," Rand Paper No. P-1662, also the 10th International Astronautical Congress, London, England, August 1959.

10. Norman Davids, and S. W. Huang, "Shock Wave Propagation in Crater Formation," Technical Report No. 2, Research Grant NsG-66-60, Department of Engineering Mechanics, Pennsylvania State University, 1960.

11. M. J. P. Musgrave, "The Propagation of Elastic Waves in Crystals and Other Anisotropic Media," Reports on Progress in Physics, Vol. XXII, p. 74, 1959.

12. R. B. Lindsay, Mechanical Radiation, McGraw-Hill Book Company, Inc., New York, 1960.

13. R. B. Clay, M. A. Cook. R. T. Keyes, "Formation and Behavior of Shock Waves in Solids," Technical Report, Contract Nord-17371, Institute of Metals and Explosives Research, University of Utah, 1960.

14. M. P. White and L. Griffis, "Propagation of Plasticity in Uniaxial Compression," A.S.M.E. Trans.,Vol. 70, Jour. Appl. Mechanics, Vol. 15, pp. 256, 1948.

15. D. S. Wood, "On Longitudinal Plane Waves of Elastic-Plastic Strain in Solids," A.S.M.E. Trans., Vol. 74, Jour. Appl. Mechanics, Vol. 19, p. 521, 1952.

16. T. F. Heuter and R. H. Bolt, Sonics, John Wiley and Sons, Inc., New York, 1955.

17. Electro-Ceramics, Inc., 2645 South 2nd West, Salt Lake City, Utah.

18. W. P. Mason, Piezoelectric Crystals and Their Application to Ultrasonics, D. Van Nostrand Company, Inc., New York, 1950, Chapter 12.

19. ALCOA Structural Handbook, Aluminum Company of America, Pittsburgh, Pennsylvania, p. 36.

20. American Institute of Physics Handbook, McGraw-Hill Book Company, Inc., New York, 1957, p. 3-81, p. 3-95.

21. Skinner and Phillips, The Science of Dental Materials, Saunders, Inc., Philadelphia, Pennsylvania.

22. N. O. Taylor, W. T. Sweeney, D. B. Mahler, and E. J. Dinger, "The Effects of Variable Factors on Crushing Strengths of Dental Amalgams," Jour. of Dental Research, Vol. 28, p. 228, June, 1949.

23. J. Marx, "Use of Piezoelectric Gage for Internal Friction Measurements," Rev. Sci. Inst., Vol. 22, p. 503, 1951.

24. J. L. Seely, "Pressure Effects on the Internal Friction of Aluminum," Ph.D. Thesis, University of Utah, 1962.

25. Hartford Steel Ball Co., Inc., Hartford 6, Conn.

26. Glasoe and Lebacqz, Pulse Generators, M.I.T. Radiation Lab Series, p. 666 ff.

27. Melvin Brown, "Transient Analysis of the White Cathode Follower," Rev. Sci. Inst., Vol. 31, p. 403, April, 1960.

28. National Metalizing Corp. 825 New York Avenue, Trenton 8, New Jersey.

29. Neil P. Bailey, C. Eugene McDermott, Dietrich K. Gehmlich, and E. P. Palmer, "Hyper-Elastic Impacts," Technical Report UU-8 on Contract AF 04(647)-942, High Velocity Laboratory, University of Utah, 1962.

30. Radiotron Designer's Handbook, edited by F. Langford-Smith, Amalgamated Wireless Valve Company Pty. Ltd., Sydney, Australia, 1952, p. 400. Thirty-two references are listed.

31. E. L. C. White, U. S. Patent No. 2,358,428, September 19, 1944.

32. Melvin Brown, "Greater Gain Band Width in Trigger Circuits," Rev. Sci. Inst., Vol. 30, p. 169, March, 1959.

33. Phillip L. Read, "Ultralinear Cathode Follower," Rev. Sci. Inst., Vol. 31, p. 979, September, 1960.

34. ENSCO Engineering Specialty Co., 3100 Eldredge Street, Salt Lake City 15, Utah.

AD-

University of Utah, High-Velocity Laboratory, Salt Lake City, Utah.
STRESS-TIME MEASUREMENTS IN HIGH VELOCITY IMPACT by S.M. Taylor, E.P. Palmer, and R.R. Kadesch. July 1963, 78 p. illus. tables.
(Technical Report UU-13
BSD-TDR-63-178)
Unclassified Report

A new method for the measurement of stress-time effects in high velocity impact is outlined. A technique for
(over)

UNCLASSIFIED

1. Wave Propagation Theory, Measurements
2. $BaTiO_3$ transducer properties
I. Taylor, S.M. Palmer, E.P. Kadesch,R.R.

UNCLASSIFIED

AD-

University of Utah, High-Velocity Laboratory, Salt Lake City, Utah.
STRESS-TIME MEASUREMENTS IN HIGH VELOCITY IMPACT by S.M. Taylor, E.P. Palmer, and R.R. Kadesch. July 1963, 78 p. illus. tables.
(Technical Report UU-13
BSD-TDR-63-178)
Unclassified Report

A new method for the measurement of stress-time effects in high velocity impact is outlined. A technique for
(over)

UNCLASSIFIED

1. Wave Propagation Theory,Measurements
2. $BaTiO_3$ transducer properties
I. Taylor, S.M. Palmer, E.P. Kadesch,R.R.

UNCLASSIFIED

AD-

University of Utah, High-Velocity Laboratory, Salt Lake City, Utah.
STRESS-TIME MEASUREMENTS IN HIGH VELOCITY IMPACT by S.M. Taylor, E.P. Palmer, and R.R. Kadesch. July 1963, 78 p. illus. tables.
(Technical Report UU-13
BSD-TDR-63-178)
Unclassified Report

A new method for the measurment of stress-time effects in high velocity impact is outlined. A technique for
(over)

UNCLASSIFIED

1. Wave Propagation Theory, Measurements
2. $BaTiO_3$ transducer properties
I. Taylor, S.M. Palmer, E.P. Kadesch,R.R.

UNCLASSIFIED

AD-

University of Utah, High-Velocity Laboratory, Salt Lake City, Utah.
STRESS-TIME MEASURMENTS IN HIGH VELOCITY IMPACT by S.M. Taylor, E.P. Palmer, and R.R. Kadesch. July 1963, 78 p. illus. tables.
(Technical Report UU-13
BSD-TDR-63-178)
Unclassified Report

A new method for the measurement of stress-time effects in high velocity impact is outlined. A technique for
(over)

UNCLASSIFIED

1. Wave Propagation Theory,Measurements
2. $BaTiO_3$ transducer properties
I. Taylor, S.M. Palmer, E.P. Kadesch,R.R.

UNCLASSIFIED

AD- UNCLASSIFIED

mounting small barium titanate piezo-electric transducers within semi-infinite aluminum targets is described. The electronic circuitry is shown. The use of isotropic elastic theory to analyze the data demonstrates that the experimental technique is a suitable method for the measurement of these phenomena. It is demonstrated that the method will give significant information about wave propagation and stress levels in elastic and plastic waves.

II. Air Force Ballistic Systems Division Air Force Systems Command

III. Contract AF 04 (694)-259

UNCLASSIFIED

AD- UNCLASSIFIED

mounting small barium titanate piezo-electric transducers within semi-infinite aluminum targets is described. The electronic circuitry is shown. The use of isotropic elastic theory to analyze the data demonstrates that the experimental technique is a suitable method for the measurement of these phenomena. It is demonstrated that the method will give significant information about wave propagation and stress levels in elastic and plastic waves.

II. Air Force Ballistic Systems Division Air Force Systems Command

III. Contract AF 04 (694)-259

UNCLASSIFIED

AD- UNCLASSIFIED

mounting small barium titanate piezo-electric transducers within semi-infinite aluminum targets is described. The electronic circuitry is shown. The use of isotropic elastic theory to analyze the data demonstrates that the experimental technique is a suitable method for the measurement of these phenomena. It is demonstrated that the method will give significant information about wave propagation and stress levels in elastic and plastic waves.

II. Air Force Ballistic Systems Division Air Force Systems Command

III. Contract AF 04 (694)-259

UNCLASSIFIED

AD- UNCLASSIFIED

mounting small barium titanate piezo-electric transducers within semi-infinite aluminum targets is described. The electronic circuitry is shown. The use of isotropic elastic theory to analyze the data demonstrates that the experimental technique is a suitable method for the measurement of these phenomena. It is demonstrated that the method will give significant information about wave propagation and stress levels in elastic and plastic waves

II. Air Force Ballistic Systems Division Air Force Systems Command

III. Contract AF 04 (694)-259

UNCLASSIFIED

UNCLASSIFIED